Trigger studies for the future neutrino telescope ORCA

Diplomarbeit

vorgelegt von
Tamás Gál aus Debrecen

Erlangen Centre for Astroparticle Physics
Physikalisches Institut I
Friedrich-Alexander-Universität
Erlangen-Nürnberg

1. Gutachter: Prof. Dr. Uli Katz
2. Gutachter: Dr. Thomas Eberl

Tag der Abgabe: 31. 07. 2013

Contents

1 Introduction **3**

1.1 Neutrino Oscillations 4

1.1.1 Neutrino Oscillations in Vacuum 5

1.1.2 Neutrino Oscillations in Matter 6

1.2 The Neutrino Mass Hierarchy Problem 8

2 The ORCA Detector **9**

2.1 Detection Principle 10

2.2 Sources of Cherenkov Light 11

2.3 Detector Layout 13

2.4 Optical Module 15

2.5 Photomultiplier Tubes 16

3 Simulations **18**

3.1 Event Generators 18

3.1.1 GENIE 18

3.1.2 gSeaGen 19

3.1.3 Mupage 19

3.2 Photon Propagation 19

3.2.1 GEASIM 20

3.2.2 KM3 20

3.2.3 CLSim 20

3.3 Potassium-40 Noise 21

3.4 Muon Track Reconstructions via FilteringFit 21

4 Event Selection **22**

4.1 Contained Events 22

4.2 Premium Events 23

4.3 Reconstructed Events 24
4.4 Atmospheric Muon Background Events 25

5 Trigger **26**
5.1 Signal Analysis 27
5.1.1 OM Pulse Statistics 27
5.1.2 Intra OM Pulses 34
5.1.3 PMT Hit Coincidence Times 34
5.2 Trigger Algorithms 37
5.2.1 Trigger TnOMm 37
5.2.2 Trigger TnSm 38
5.3 Evaluation of Trigger Performance 39
5.3.1 Purity 39
5.3.2 Trigger Efficiencies 40
5.3.3 Trigger Efficiencies on Reconstruction Level 49
5.3.4 Trigger Rates 50

6 Summary and Outlook **51**

Bibliography **55**

List of Figures **57**

List of Tables **58**

Chapter 1

Introduction

Recent measurements of a large neutrino mixing angle θ_{13} have substantially enhanced the interest of physicists in the measurement of CP-violation in the lepton sector. ORCA is a future deep sea neutrino detector with the aim of making a neutrino mass hierarchy determination — an important parameter for future CP-violation experiments — by measuring the flux of low energy atmospheric neutrinos.

The purpose of this study is to introduce low level trigger algorithms for the ORCA detector and evaluate the trigger efficiencies on Monte Carlo simulations. After a short theoretical journey through the mysterious oscillation properties of neutrinos, the ORCA neutrino detector and its detection principle are described. The next chapter gives a brief overview of the software tools used to generate the Monte Carlo simulations for the trigger studies in this thesis. The generated events and the event selection criteria are then presented, followed by the final chapter which discusses the signal analysis, trigger algorithms and the performance of different trigger configurations.

1.1 Neutrino Oscillations

The first experiment to measure the flux of neutrinos from the Sun was started in the late 1960s by Ray Davis and John N. Bahcall in the Homestake Gold Mine in Lead, South Dakota. The idea was to extract and count radioactive isotopes of argon, which were created upon collisions of solar neutrinos with chlorine atoms in a target medium. Since the cross section of neutrino-nucleon interactions is extremely small [13], a huge target was needed. A 380 m³ tank of tetrachlorethylene (C_2Cl_4) was placed nearly 1500 m below underground to suppress the intense flux of energetic particles produced by cosmic rays. To catch the argon that had formed due to neutrino-chlorine interactions, the tank had to be "bubbled out" with helium every few weeks. It was an exceptionally challenging undertaking, but it has been shown that apparently only about one-third to one half of the neutrinos predicted by models of the solar interior reaches the Earth. First responds were that either Bahcall, who made the theoretical work, or Davis, who designed the actual experiment had made a mistake, but both the theoretical model and the experiment were checked, with no errors found. Several other experiments with the same purpose followed (Kamiokande[1], Super Kamiokande[2], SAGE[3], GALLEX[4] etc.) and this "neutrino deficit" became known as the **solar neutrino problem**.

Although the Super-K results from 1998 have already shown evidence for neutrino oscillations[19], the final conclusion that neutrinos change their flavour as they travel from the Sun to the Earth was published by the Sudbury Neutrino Observatory (SNO) on 18 June 2001 [1].

Until today, solar experiments confirmed oscillations from $\nu_e \rightarrow \nu_{\mu,\tau}$, measurements of neutrinos from nuclear reactors showed $\not{\nu}_e \rightarrow \not{\nu}_{other}$ and accelerator experiments also covered the $\nu_\mu \rightarrow \nu_{other}$ transitions. In 2013 — and twice before in 2010 [3] and in 2012 — the OPERA experiment at the INFN Gran Sasso Laboratory in Italy has also observed a tau neutrino candidate from flavour oscillation [8]. The muon neutrino, which was produced at CERN in Geneva changed flavour on its way to the

[1]Kamioka Underground Observatory: http://www-sk.icrr.u-tokyo.ac.jp/kam/kamiokande.html

[2]Super-Kamiokande experiment: http://www-sk.icrr.u-tokyo.ac.jp/sk/index-e.html

[3]SAGE (Soviet-American Gallium Experiment): http://ewi.npl.washington.edu/sage

[4]GALLEX: a radiochemical GALLium EXperiment to detect solar pp neutrinos http://www.mpi-hd.mpg.de/lin/research_history.en.html

Gran Sasso laboratory and arrived as a tau neutrino [8]. These observations also imply that neutrinos have distinct masses and obviously mix.

1.1.1 Neutrino Oscillations in Vacuum

The flavour eigenstates $|\nu_\alpha\rangle$ (i.e., ν_e, ν_μ and ν_τ) differ from the mass eigenstates $|\nu_j\rangle$ (i.e., ν_1, ν_2 and ν_3) for massive neutrinos. The transformations between these eigenstates are written by

$$|\nu_\alpha\rangle = \sum_j U_{\alpha j}|\nu_j\rangle \quad \text{resp.} \quad |\nu_j\rangle = \sum_\alpha U^+_{j\alpha}|\nu_\alpha\rangle = \sum_\alpha U^!_{j\alpha}|\nu_\alpha\rangle \tag{1.1}$$

where $U_{\alpha j}$ are the elements of the unitary transformation matrix U between mass eigenstates and flavour eigenstates, so

$$U^+ U = 1 \quad , \quad \Rightarrow \quad \sum_j U_{\alpha j} U^!_{\beta j} = \delta_{\alpha\beta} \ , \quad \sum_\alpha U_{\alpha j} U^!_{\alpha j} \ . \tag{1.2}$$

The time evolution of states is given by the Schrödinger equation:

$$i\frac{d}{dt}|\nu_j\rangle = E_j|\nu_j\rangle \ , \tag{1.3}$$

where E_j is the energy of ν_j. Since neutrino masses are sufficiently smaller than their momenta, the following approximation can be used:

$$E_j = \sqrt{p^2 + m_j^2} \approx p + \frac{m_i^2}{2p} \approx E + \frac{m_i^2}{2E} \ . \tag{1.4}$$

The solution for the neutrino wave function is

$$|\nu_j(t)\rangle = e^{iE_j t}|\nu_j(0)\rangle \ . \tag{1.5}$$

Since neutrinos are generated as a flavour eigenstate via the weak decay of particles and are observed as a flavour eigenstate in weak interactions, the initial and final states are both flavour eigenstates. Taking this into account, the Schrödinger equation Eq. (1.3) can be rewritten using Eq. (1.1) as

$$i\frac{d}{dt}|\nu_\alpha\rangle = U_{\alpha j} E_j U^!_{j\alpha}|\nu_\alpha\rangle \tag{1.6}$$

and its solution (Eq. (1.5)) is then:

$$|\nu_\alpha(t)\rangle = U_{\alpha j} e^{-iE_j t} U^{\dagger}_{j\alpha} |\nu_\alpha(0)\rangle \ . \tag{1.7}$$

The time dependent detection probability of a neutrino (ν_α) generated at $t = 0$ is given by

$$P_{\nu_\alpha \to \nu_\alpha} = |\langle \nu_\alpha(t) | \nu_\alpha(0)\rangle|^2 = \left|\langle \nu_\alpha(0) | U_{\alpha j} e^{-iE_j t} U^{\dagger}_{j\alpha} | \nu_\alpha(0)\rangle\right|^2 \ . \tag{1.8}$$

Using the approximations for E_j and p as shown in Eq. (1.4), and $t \approx L$ (in natural units), the transition probabilities of neutrinos propagating through the vacuum can be calculated. In the end, the oscillation rate depends on squared mass differences between the mass eigenstate ($\Delta m^2_{ij} = m^2_i - m^2_j$), the neutrino energy E_ν, the distance L between source and detector and the mixing angles $0 < \theta_i \leq \frac{\pi}{2}$ in the mixing matrix U:

$$U = \begin{pmatrix} 1 & 0 & 0 \\ 0 & c_2 & s_2 \\ 0 & -s_2 & c_2 \end{pmatrix} \cdot \begin{pmatrix} c_1 & s_1 & 0 \\ -s_1 & c_1 & 0 \\ 0 & 0 & 1 \end{pmatrix} \cdot \begin{pmatrix} 1 & 0 & 0 \\ 0 & 1 & 0 \\ 0 & 0 & e^{i\delta} \end{pmatrix} \cdot \begin{pmatrix} 1 & 0 & 0 \\ 0 & c_3 & s_3 \\ 0 & -s_3 & c_3 \end{pmatrix} \tag{1.9}$$

$$= \begin{pmatrix} c_1 & s_1 c_3 & s_1 s_3 \\ -s_1 c_2 & c_1 c_2 c_3 - s_2 s_3 e^{i\delta} & c_1 c_2 s_3 + s_2 c_3 e^{i\delta} \\ s_1 c_2 & -c_1 c_2 c_3 - s_2 s_3 e^{i\delta} & -c_1 c_2 s_3 + s_2 c_3 e^{i\delta} \end{pmatrix} , \tag{1.10}$$

where $s_i = \sin\theta_i$, $c_i = \cos\theta_i$ and δ is the CP-violating phase ($-\pi \leq \delta \leq \pi$).

The formulae for the calculations in this section follow [2] and [13].

1.1.2 Neutrino Oscillations in Matter

The first theory describing neutrino oscillations in matter was published in 1978 by L.Wolfenstein [21]. An electron (anti)neutrino propagating through matter is exposed to an additional potential energy of

$$V_e = (-) + \sqrt{2} G_F N_e \ , \tag{1.11}$$

(where G_F is the Fermi coupling constant and N_e the electron density) due to a (s)t-channel exchange of a W-boson, which is not present for other neutrino flavours. The interaction cross sections for different neutrino flavours are accordingly different as they pass through matter. Extending Eq. 1.6 with this potential, the neutrino propagation in matter is given as

$$i\frac{\mathrm{d}}{\mathrm{d}t}|\nu_\alpha\rangle = (U_{\alpha j}E_j U^{\dagger}_{j\alpha} + V_e)|\nu_\alpha\rangle \ . \tag{1.12}$$

The total Hamiltonian then is diagonal neither in the flavour basis nor in the vacuum mass eigenstate basis which ultimately allows transitions of $\nu_i \leftrightarrow \nu_j$ (i, j = 1, 2, 3). The important effect is that the squared mass differences in matter are shifted with respect to those in vacuum. As neutrino oscillations depend upon these mass differences, the oscillation probability in matter is different than it is in vacuum. When neutrinos travel through Earth, they experience the electron densities inside it. For neutrino energies above 2 GeV the effect is quite small for the small mass difference [13, c13], but significantly better for the neutrino mixing of the first and third mass eigenstate. The effective mass difference $\Delta m^2_{13,eff}$ of these masses in matter can be written as

$$\Delta m^2_{13,eff} = \Delta m^2_{13,vac}\sqrt{\left(\cos(2\theta_{13}) - \frac{2V_e E_\nu}{\Delta m^2_{13,vac}}\right)^2 + \sin^2(2\theta_{13})} \ . \tag{1.13}$$

Mikheyev, Smirnov and Wolfenstein showed [21][16] that this gives a rise to an oscillation resonance (MSW effect) for

$$\frac{2V_e E_\nu}{\Delta m^2_{13,vac}} = \cos(2\theta_{13}) \ . \tag{1.14}$$

The resonance condition regarding the neutrino energy is consequently given by:

$$E^{\$}_\nu = \frac{\cos(2\theta_{13})\Delta m^2_{13,vac}}{2V_e} = \pm\frac{\cos(2\theta_{13})\Delta m^2_{13,vac}}{2\sqrt{2}G_F N_e} \ . \tag{1.15}$$

This is obviously only possible for either normal mass hierarchy (+) and positive Δm^2_{13} or inverted mass hierarchy (−) and negative Δm^2_{13}.

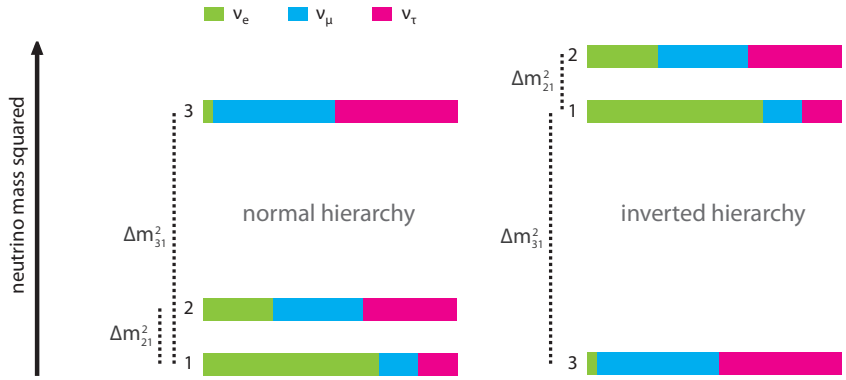

Figure 1.1: *The relationship between the neutrino mass eigenstates (1, 2 and 3) and the flavour eigenstates (coloured bars to visualise the fractional contribution of each neutrino flavour). While solar neutrinos indicate that $m_2 > m_1$[18], there is no information about m_3. If m_3 is greater than m_1 and m_2, the mass hierarchy is "normal", otherwise "inverted". (after a figure by S. Parke [15])*

1.2 The Neutrino Mass Hierarchy Problem

Although oscillation experiments cannot determine the absolute value of the neutrino masses, the sign of the mass difference ! m^2 can be measured. Due to matter effects in the Sun, measurements [18] of the sign of the mass difference ! $^2_{21}$ between the first and second mass eigenstate pointed out that $m_2 > m_1$. As a result there are two possibilities for the neutrino mass hierarchy, namely normal hierarchy (NH): $m_1 < m_2 < m_3$ and inverted hierarchy (IH): $m_3 < m_1 < m_2$ as shown in Fig. 1.1.

Chapter 2

The ORCA Detector

Determining the neutrino mass hierarchy has become a major challenge for particle physicists. To measure the effects of matter on neutrino oscillations as described in the previous chapter, a preferably dense (in terms of electron density) medium and huge detector volume is needed.

ORCA (*O*scillation *R*esearch with *C*osmics in the *A*byss) — as a phase I experiment for the KM3NeT[1] project — is a future multi-megaton Cherenkov neutrino detector in the Mediterranean Sea with the aim of detecting atmospheric neutrinos traveling through Earth.

Since the Earth's (electron) density is not homogeneous, but primarily depends on the distance to its centre [10], the electron density along a neutrino track is correlated with its location. The oscillation probabilities for atmospheric neutrinos flying through Earth being eventually detected by ORCA at the sea ground, are consequently (and again, primarily) defined by their zenith angle. Measuring the zenith angle of such a neutrino automatically refers to the electron density along its path, let alone the probabilities of changing its flavour.

[1] KM3NeT: A multi-km^3 sized Neutrino Telescope. http://www.km3net.org

2.1 Detection Principle

ORCA is a Cherenkov detector, so-called since it measures Cherenkov radiation, emitted when charged particles pass through a medium at a velocity greater than the speed of light in that medium. Although neutrinos have no electric charge, they can interact with matter via the weak-force and create charged leptons, which again emit Cherenkov radiation if their energy is above a certain threshold. The Cherenkov light emitted by such particles forms a cone with an opening angle θ_C which can be calculated by the formula

$$\theta_C = \arccos\left(\frac{1}{\beta \cdot n}\right) \ , \tag{2.1}$$

where β is the ratio of the particle's speed to the speed of light c and n the refraction index of the medium. For highly relativistic particles ($\beta \approx 1$) in sea water with $n_{sea} \approx 1.35$, the Cherenkov angle becomes $\theta_C = 42^{\circ}$.

The approximate number of Cherenkov photons per path length x emitted by a charged particle is

$$\frac{\mathrm{d}^2 N}{\mathrm{d}x\,\mathrm{d}\lambda} = \frac{2\pi\alpha}{\lambda^2}\left(1 - \frac{1}{n^2\beta^2}\right) \tag{2.2}$$

where α is the fine-structure constant, λ the Cherenkov photon's wavelength, n the refraction index of the medium and β the ratio of the particles speed to the speed of light. Since water is only transparent in a quite narrow band within the visible spectrum, the average number of photons per traveled distance is circa

$$\frac{\mathrm{d}N}{\mathrm{d}x} = 3.4 \cdot 10^4\,\mathrm{m}^{-1} \ . \tag{2.3}$$

These photons are then measured via thousands of photomultiplier tubes, which are sensitive to the corresponding electromagnetic spectrum (see 2.5 for more details).

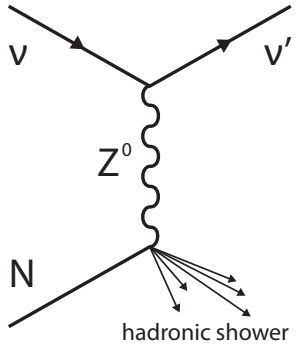

Figure 2.1: *The NC neutrino interaction channel visible for neutrino telescopes.*

2.2 Sources of Cherenkov Light

There are two types of neutrino interactions: neutral current (NC) and charged current (CC) interaction. These channels can be formulated as

$$\nu_l + N \rightarrow l^+ + X \quad \text{resp.} \quad \bar{\nu}_l + N \rightarrow l^- + X \quad (CC) \tag{2.4}$$

and

$$\nu_l + N \rightarrow \nu_l + X \quad \text{resp.} \quad \bar{\nu}_l + N \rightarrow \bar{\nu}_l + X \quad (NC), \tag{2.5}$$

where ν_l and $\bar{\nu}_l$ represent the neutrino and anti-neutrino with flavour l, l^- and l^+ the charged lepton and anti-lepton, N is the nucleus and X the hadronic shower.

In NC interactions a neutrino — with the same flavour as the incoming neutrino — and a hadronic shower are produced (see Fig. 2.1). Whereas the hadronic shower produces Cherenkov light, the produced neutrino remains invisible to the detector, unless it instantly interacts within the detector volume which is quite unlikely.

In the following the origins of the Cherenkov photons in CC interactions are discussed.

CC Interactions

The lepton created in the CC channel can be either an electron, muon or tau (respectively positron, antimuon or antitau). While in each case a hadronic shower is created at the interaction vertex, further development of the process differs (see

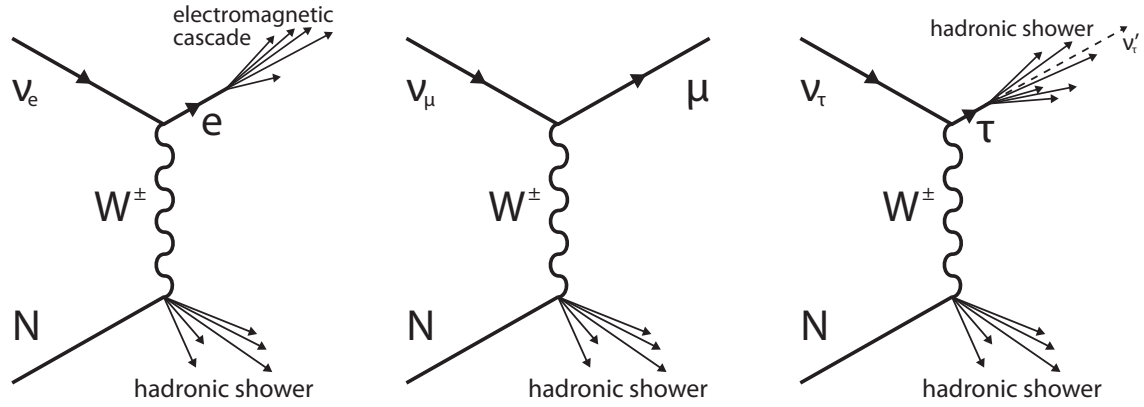

Figure 2.2: *The neutrino CC interactions relevant for neutrino telescopes: the left one shows the production of $e^\pm$ and an electromagnetic cascade, the middle one the creation of a $\mu^\pm$ and the right one the $\tau^\pm$ with its double-bang signature (two hadronic showers).*

Fig. 2.2).

Electrons and positrons with a high energy ($> 10\,\mathrm{MeV}$) primarily emit photons (bremsstrahlung), which on the other hand produce electron-positron pairs (pair production). These two processes continue until the photons energies fall below the pair production threshold. The radiation length[2] for a medium consisting of a single type of element can be approximated by the following analytical formula[20]:

$$X_0 = \frac{716{,}405 \cdot A}{Z(Z+1)\ln\left(\frac{287}{\sqrt{Z}}\right)} \cdot \mathrm{g} \cdot \mathrm{cm}^{-2} \,, \tag{2.6}$$

where A is the mass number of the nucleus and Z is the atomic number. For a composite material (like water), the radiation length $X_{0,comp}$ can be estimated by the formula

$$X_{0,comp} = \frac{W_0}{\sum \frac{W_i}{X_i}} \,, \tag{2.7}$$

where W_0 is the total mass of the sample, W_i the mass and X_i the radiation length of the individual components. The radiation length of (liquid) water according to PDG[3] is $X_{0,H_2O} = 36.08\,\mathrm{g} \cdot \mathrm{cm}^{-2}$, thus the overall length of an electromagnetic shower in water caused by an electron or positron with energies below $\approx 20\,\mathrm{GeV}$ is commonly less than a few meters. The hadronic cascade at the interaction vertex is

[2]The radiation length is defined for electrons as the length over which the energy of the electron is reduced by the factor $\frac{1}{e}$, while for photons it is defined as $\frac{7}{9}$ of the mean free path. Although it is measured in $\mathrm{g} \cdot \mathrm{cm}^{-2}$, the characteristic length can be obtained by multiplying it by the density of the material.

[3]http://pdg.lbl.gov/2009/AtomicNuclearProperties/HTML_PAGES/276.html

superposed by such electromagnetic cascades.

In case of a **muon or antimuon**, the energy loss due to bremsstrahlung is significantly lower, hence the track length is much longer. A rule of thumb for the track length of a muon (or antimuon) with the energy of $E_\mu > 1\,\mathrm{GeV}$ in water is

$$x = E_\mu \cdot \mathrm{GeV}^{-1} \cdot 4.25\,\mathrm{m}\,. \tag{2.8}$$

More accurate values can be found on the PDG website[4]. The direction of the neutrino and the muon are highly correlated. The uncertainty in the opening angle between them can be approximated as

$$\Delta\alpha_{\nu,\mu} \approx 30^\circ \cdot \sqrt{\frac{1\,\mathrm{GeV}}{E_\nu}} \tag{2.9}$$

where E_ν is the neutrino energy in GeV [14].

The third and also last possible lepton flavour in the CC channel is **tau or antitau**, with a vastly short decay time of $t_\tau = 290.6 \pm 1.0\,\mathrm{fs}$. Its main signature is the so called "double-bang" structure: a hadronic shower at the interaction vertex and a second shower due to the decay of the tau. This type of interaction is not covered in this thesis.

2.3 Detector Layout

The current ORCA reference detector for simulations consists of 50 randomly distributed strings with a mean minimum distance of $\approx 16\,\mathrm{m}$ between them. The positions of these detector units are irregular at the level of 2 m. An example footprint and the nearest distances between the strings are shown in Fig. 2.3. Each string holds 20 optical modules (OM), where the lowest one is 100 m above the seabed and the distance between the OMs is 6 m.

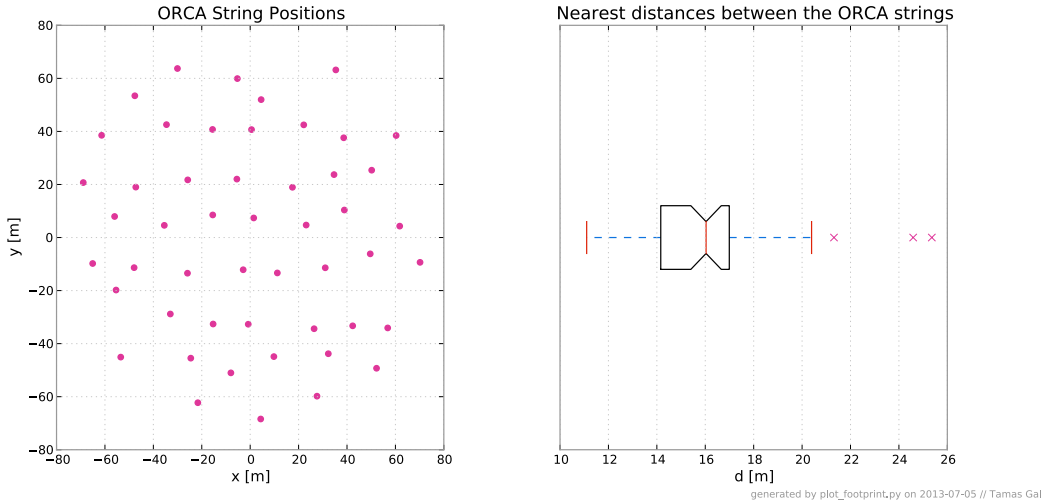

Figure 2.3: *An example footprint of the ORCA detector. The plot on the right is a boxplot of the nearest distances between the strings. The median is marked by the (red) notch of the box, the left and right side of the box is the first and third quartile of the dataset and the whiskers (red lines left and right) mark the minimum and maximum of the data not considering outliers (pink ×).*

Figure 2.4: *The optical module of the ORCA detector (photo taken from* `http://www.km3net.org`*).*

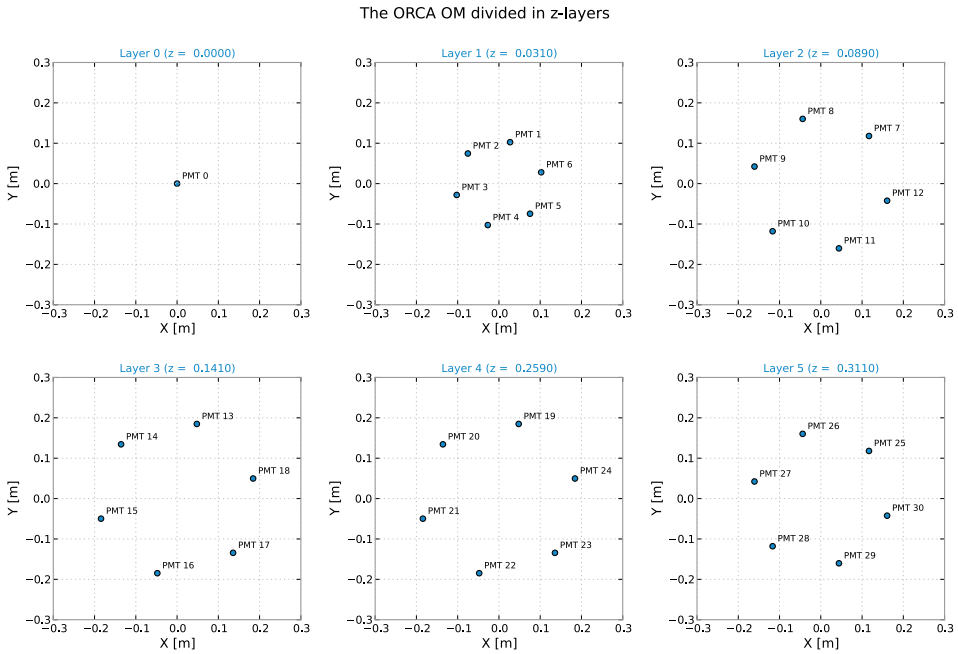

Figure 2.5: *The positions of the PMTs in the ORCA optical module.*

2.4 Optical Module

The optical module (OM) is a 17 in glass sphere containing 31 photomultiplier tubes (PMT), each with a diameter of 3 in. Fig 2.4 shows a picture of the OM. The glass sphere is filled with a gel to fight the enormous pressure under deep sea conditions[5] and hold the PMTs in place.

To get a better overview of the positions of the PMTs inside the OM, a split-up into layers in the xy-plane, as shown in Fig 2.5 is helpful. Layer 0 to 3 contain overall 19 PMTs which are "looking" downward, the upper two layers (4 and 5) with a total of 12 PMTs are oriented upward.

The exact values of the azimuth and zenith angles of each PMT are shown in Fig. 2.6.

[4] http://pdg.lbl.gov/2012/AtomicNuclearProperties/MUON_ELOSS_TABLES/muonloss_276.pdf

[5] $P_{seawater} = \rho_{seawater} \cdot g \cdot y \overset{y=2500\ m}{\approx} 250\,\mathrm{bar}$

PMT angles

azimuth / zenith	300°	330°	0°	30°	60°	90°	120°	150°	180°	210°	240°	270°
56.1°		30		25		26		27		28		29
72.8°	24		19		20		21		22		23	
107.3°		18		13		14		15		16		17
123.9°	12		7		8		9		10		11	
147.9°		6		1		2		3		4		5
180.0°	0											

Figure 2.6: *Angles between PMTs in the ORCA optical module.*

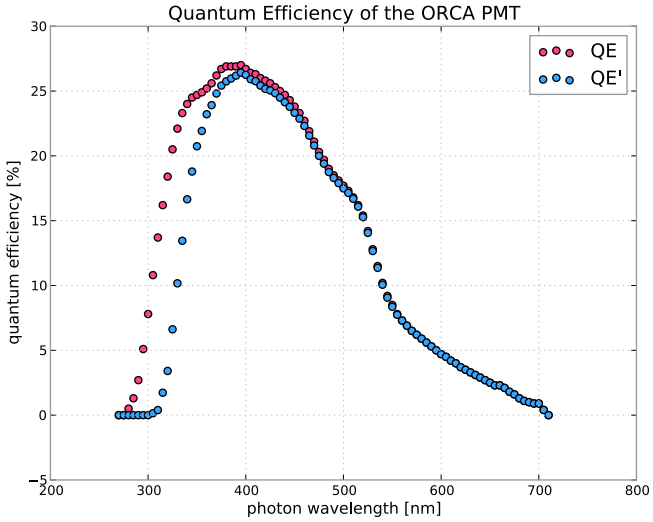

Figure 2.7: *The quantum efficiency (*QE*) of the ORCA for different photon wavelengths. The blue dots (*QE'*) represent the overall quantum efficiency including the optical transmissivity of the OM's glass sphere and the gel. The data is taken from [17].*

2.5 Photomultiplier Tubes

The eyes of ORCA and therefore probably its most important parts are the photomultiplier tubes (PMTs) as mentioned in the previous section (see 2.4). The diameter of a PMT is 76 mm (about 3 in). The quantum efficiency and the overall quantum efficiency which includes the optical transmissivity of the OM's glass sphere and the gel, are shown in Fig. 2.7. The readout scheme of the signal is a

time-over-threshold (TOT) approach. Once the PMT signal is above[6] a predefined limit, it is integrated for a certain time and the overall "time over threshold" in ns is recorded and sent to shore bundled with information about the pulse time and PMT id etc. The overall timing accuracy of the PMT readout is 2 ns.

[6] actually *below*, since a photomultiplier signal is in fact a voltage drop

Chapter 3

Simulations

In this chapter, several tools used for Monte Carlo simulations are described briefly, including neutrino and muon event generators, software packages for particle and photon propagation, a noise generator and a reconstruction package used to reconstruct muon tracks produced in CC interactions.

3.1 Event Generators

3.1.1 GENIE

GENIE [4] is a neutrino Monte Carlo (MC) generator based on ROOT[1]. Its long-term goal is to become a state-of-the-art neutrino event generator with wide applicability, hence it supports several neutrino species and nuclear targets over a broad energy range (the official versions currently support an energy range from $\approx 1\,\mathrm{MeV}$ up to $\approx 500\,\mathrm{GeV}$). The fundament for GENIE was provided by code from the SOUDAN 2 experiment [11].

[1] ROOT is an object oriented software framework designed for large scale data analysis. It is developed by CERN and published under the terms of the GPL. Visit http://root.cern.ch for more information.

3.1.2 gSeaGen

Since GENIE (see 3.1.1) is a quite complex piece of software, several wrappers have been developed to simplify its use. One of these, used in the KM3NeT collaboration, is *gSeaGen*, written and maintained by Carla Distefano[2]. *gSeaGen* consists of three parts. The first part is a flux driver, which describes the incident neutrino flux (i.e., generates a power law, computes weights for atmospheric neutrino fluxes, simulates the Earth absorption for up-going neutrino etc.). The second part is a geometry driver, which is responsible for the neutrino interaction target like interaction volume, target composition etc. The last part is the muon propagation, where muons get propagated through the target medium up to the detector, if the interaction was outside of its instrumented volume.

3.1.3 Mupage

MUPAGE a *MU*on *GE*nerator for neutrino telescopes based on *PA*rametric formulas, is used to generate the atmospheric muon background. More details about this tool can be found in [7].

3.2 Photon Propagation

Before simulating the detector response of a Cherenkov detector, i.e., the actual signal from the PMTs, particles in the generated events have to be tracked until their energies fall below the threshold, required to emit Cherenkov photons. The photons then need to be propagated through the medium until they either reach a PMT, or are being absorbed. There are two common ways to handle the photon propagation: direct tracking of the photons, which is expensive according to CPU time, or filling a lookup-table with pre-simulated data to reduce the calculation time.

[2]Instituto Nazionale di Fisica Nucleare, Laboratori Nazionali del Sud

3.2.1 GEASIM

geasim is a Monte Carlo particle tracker based on Geant3 (GEometry ANd Tracking)[3], a detector description and simulation tool originally developed at CERN. *geasim* simulates relevant physics processes for each particle using Geant3, however, it does not take into account the effects of light scattering. The advantage of this approach is reduced CPU consumption, since photons travel in straight lines and can simply be thrown away if their tracks do not cross any PMT's faceplate.

3.2.2 KM3

The *km3* package is a muon tracker and Cherenkov light propagator which uses lookup-tables to radically reduce the CPU time [6]. First, the photons are simulated with *gen*, a Geant3 based tool, which splits the muon track and the electromagnetic shower into short segments of 1-2 m. The emitted photons are then propagated through the medium, considering light absorption and scattering effects. To record photons, the dimensions of concentric spheres surrounding the simulated particles have to be defined. Every photon which intersects one or more of these shells is then passed to the next tool in the package, called *hit*, which finally writes the probability distributions of the photons into the above-mentioned lookup-tables, while it also takes into account the wavelength-dependent quantum efficiency and angular acceptance of the PMTs. The final step is using MUSIC [5] to propagate the muon and utilise the photon tables to create the actual PMT hits.

3.2.3 CLSim

Although both *geasim* and *km3* are performing well, light propagation would be far more accurate if each of the photons were handled individually, while also taking into account light absorption and scattering effects. Of course, the huge amount of photons leads to extremely high CPU consumption, thus Monte Carlo mass productions would be impractical. The good news is that photon tracking mostly consists of basic geometric calculations which can be done by simple processors and most importantly: in parallel. Since today's consumer graphic cards have several dozens

[3] http://wwwasd.web.cern.ch/wwwasd/geant/

(and often hundreds) of cores, they can be used to do the job. *CLSim*, written and maintained by Claudio Kopper, is designed to do full photon generation and tracking, with support of optional GPU acceleration using OpenCL[4]. Despite the fact that it was originally written in the SeaTray framework used for ANTARES and KM3NeT studies, the current (and unfortunately also older) code does not work anymore out of the box. Several changes have to be made to SeaTray and clsim itself to get it compiled and still, it seems not to work with the current reference detector's geometry.

3.3 Potassium-40 Noise

Besides bioluminescence — whose statistics are not included in the current simulation chains — and the atmospheric muon flux, ^{40}K-noise is part of the main signal of the ORCA detector. The noise is simulated by *modk40*, a software package which mimics the PMT hit rates due to decay of the radioactive isotope potassium-40 (^{40}K).

The configuration parameters of *modk40* for simulations used in this study, are an overall ^{40}K frequency of 5 kHz and a coincidence rate (two hits within 20 ns on an OM) of 500 Hz.

3.4 Muon Track Reconstructions via FilteringFit

FilteringFit is a full-sky scanning linear fit algorithm combined with a 2D clustering hit selection. The reconstruction of the muon track is done in multiple stages. The first step scans the sky for prefit candidates and adds several tracks in a cone around each prefit track. In the next step, fits are performed on each prefit candidate and the track with the lowest likelihood is selected. The final track is then obtained by completing a final fit on the best track. Although *FilteringFit* was originally written for ANTARES, it can be configured to work with simulations for the ORCA detector[5] and is currently one of the very few reconstruction methods available.

[4] http://www.khronos.org/opencl

[5] as shown by Robert Bormuth (Univ. Leiden) and Jannik Hofestädt (ECAP) at the ORCA workshop in Paris on 17-18th April 2013

Chapter 4

Event Selection

4.1 Contained Events

The Monte Carlo simulations for these events are produced using *km3*, *geasim*, and *modk40*. A *contained event* is defined as a muon neutrino CC interaction, where the muon's track is completely contained within the instrumented volume with an optional *safety margin*. To shape the contained volume, a convex hull algorithm

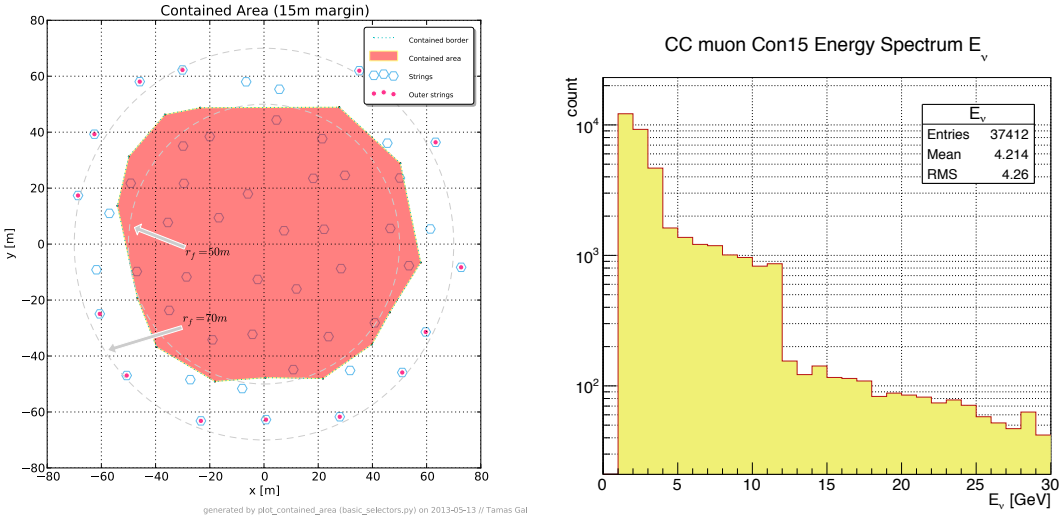

Figure 4.1: *The contained area/volume definition (left) and the energy spectrum of the neutrinos in contained CC muon events (right).*

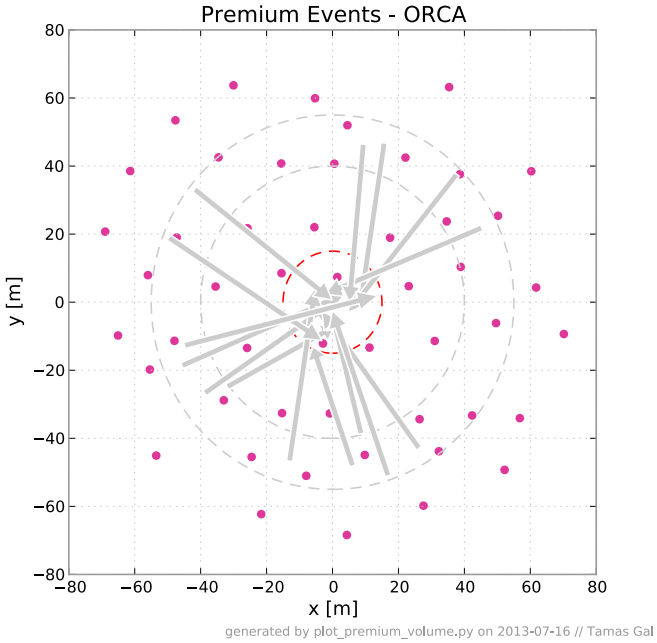

Figure 4.2: *The premium event definition (left) in the ORCA reference detector. The bounds of the outer sphere are* $R_{min} = 40\,\mathrm{m}$ *and* $R_{max} = 55\,\mathrm{m}$*, the radius of the inner sphere is* $R_{centre} = 15\,\mathrm{m}$*. The xy-plane is in the middle of the detector. The interaction vertices are located between the two concentric spheres and the track of the muon is pointing toward the smaller sphere in the middle of the instrumentation volume.*

[12][1] is used to determine the positions of the boundary OMs. The resulting volume is then shrunk by a given value. Fig. 4.1 shows the contained volume or rather area—which extends to a volume in the z-direction—with a safety margin of 15 m. The unweighted energy spectrum of the neutrinos in contained CC muon events is shown in Fig. 4.1.

4.2 Premium Events

The simulation chain used for these Monte Carlo simulations is the same as for contained events (*km3*, *geasim*, and *modk40*) although a more stringent definition of containment, so-called *premium event* was proposed[2] and later presented by Jannik

[1] Calculating the positions of the outermost OMs in the xy-plane—i.e., using a 2D convex hull algorithm—is sufficient, since the x and y coordinates of the OM are the same on each string.

[2] ORCA mailing list from 22nd June 2013 http://listserv.in2p3.fr/cgi-bin/wa?A2=ORCA-L;e8eb66c4.1306

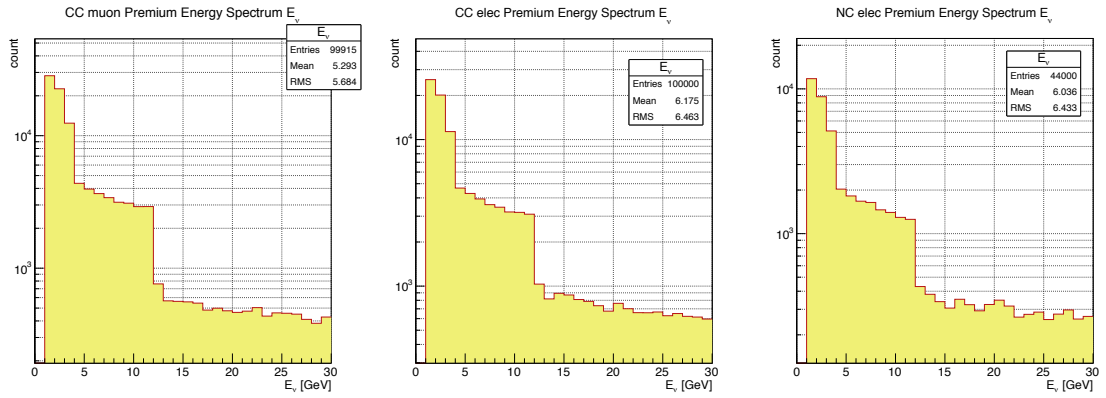

Figure 4.3: *The generated energy spectra of the neutrinos in contained CC muon and CC/NC electron events.*

Hofestädt[3] at an ORCA telephone conference on 11th July 2013:

> *Premium Events:* Events, where all produced light is (nearly) contained in the instrumented volume i.e., only a negligible amount of photons escapes the instrumented volume. Since for mass hierarchy determination the up-going events (neutrino zenith angle $>$ 90°) are the most valuable ones, only those are counted as premium events.

Fig. 4.2 illustrates the premium events definition in the xy-plane at $z = \frac{h_{string}}{2}$.

4.3 Reconstructed Events

This data sample consists of premium CC muon events, which were reconstructed using *FilteringFit*. Only those events were selected, where the angular distance between the reconstructed muon and the simulated muon is better than 5 degrees Only such events were used in this thesis to determine the efficiency of different trigger configurations on reconstruction level.

[3]Erlangen Centre for Astroparticle Physics (ECAP)

4.4 Atmospheric Muon Background Events

These events contain bundles of atmospheric muons/anti-muons simulated with *MUPAGE* and noise from ^{40}K decay via the *modk40* package. An overall lifetime of $\approx 25.7\,\mathrm{d}$ was available to estimate and study the trigger rates for the ORCA detector.

Chapter 5

Trigger

The approximate daily data output amount of the ORCA reference detector with its 31000 PMTs at an assumed average noise rate — mainly due to potassium decays and bioluminescence — of 5 kHz (including dark current) per PMT and 6 bytes for each encoded pulse is ≈ 73 TByte. This estimate only covers pure pulse information.

To separate the wheat from the chaff some filters, so-called triggers need to be applied, since the fraction of interesting physics events is quite low compared to the overall output size. Such trigger algorithms look for patterns in the signal stream and decide whether there is an event worth to be written out. In this vein the amount of data can be reduced to manageable levels.

This chapter describes the characteristics of the detector signal and introduces flexible trigger algorithms. The efficiencies and rates of different trigger configurations are then investigated using different Monte Carlo simulations, including pure noise events, real physics events, reconstructed events and atmospheric muon events.

5.1 Signal Analysis

In order to develop trigger algorithms and optimise their parameters, the detector signal has to be analysed thoroughly. In the following, pulse distributions and statistics for simulated contained and premium events with and without noise are presented. A *pulse* in this section is defined as a so-called L0-hit (from the level zero signal processing with an accuracy of 1 ns), which is a calibrated raw hit with $> 0.3pe$.

5.1.1 OM Pulse Statistics

OMs Hit per Event

One interesting parameter is the total number of OMs with at least one pulse per event. Since the total number of Cherenkov photons generated by a cascade or a charged lepton is highly correlated with the primary particle's energy, an increasing number of hit OMs is expected for higher neutrino energies.

Fig. 5.1 shows the number of OMs hit vs. the primary neutrino's total energy. The data was generated from 37k contained muon CC events and 100k premium events without noise. The upper two plots show the hit statistics for contained events. The vertical lines at about 3.5 GeV and 12 GeV are due to the discrete energy spectrum of the generated events (see 4.3). Same kind of statistics for 100k premium muon CC events is shown in the middle two plots. The vertical voids are the results of the neutrino event generation, where the neutrino energies were not evenly distributed but in energy bins of

$$(i - 0.1)\text{GeV} < E_{\nu,i} < (i + 0.1)\text{GeV} \quad , \quad \text{with } i \in \mathbb{N}.$$

The linear dependence of the total numbers of OMs hit and the primary neutrino energy for energies below $\approx 15\,\text{GeV}$ is readily identifiable in both graphs. The according statistics for each neutrino energy bin is shown in Fig. 5.1 in the bottom two graphs as a series of box plots. The medians are represented by the red lines,

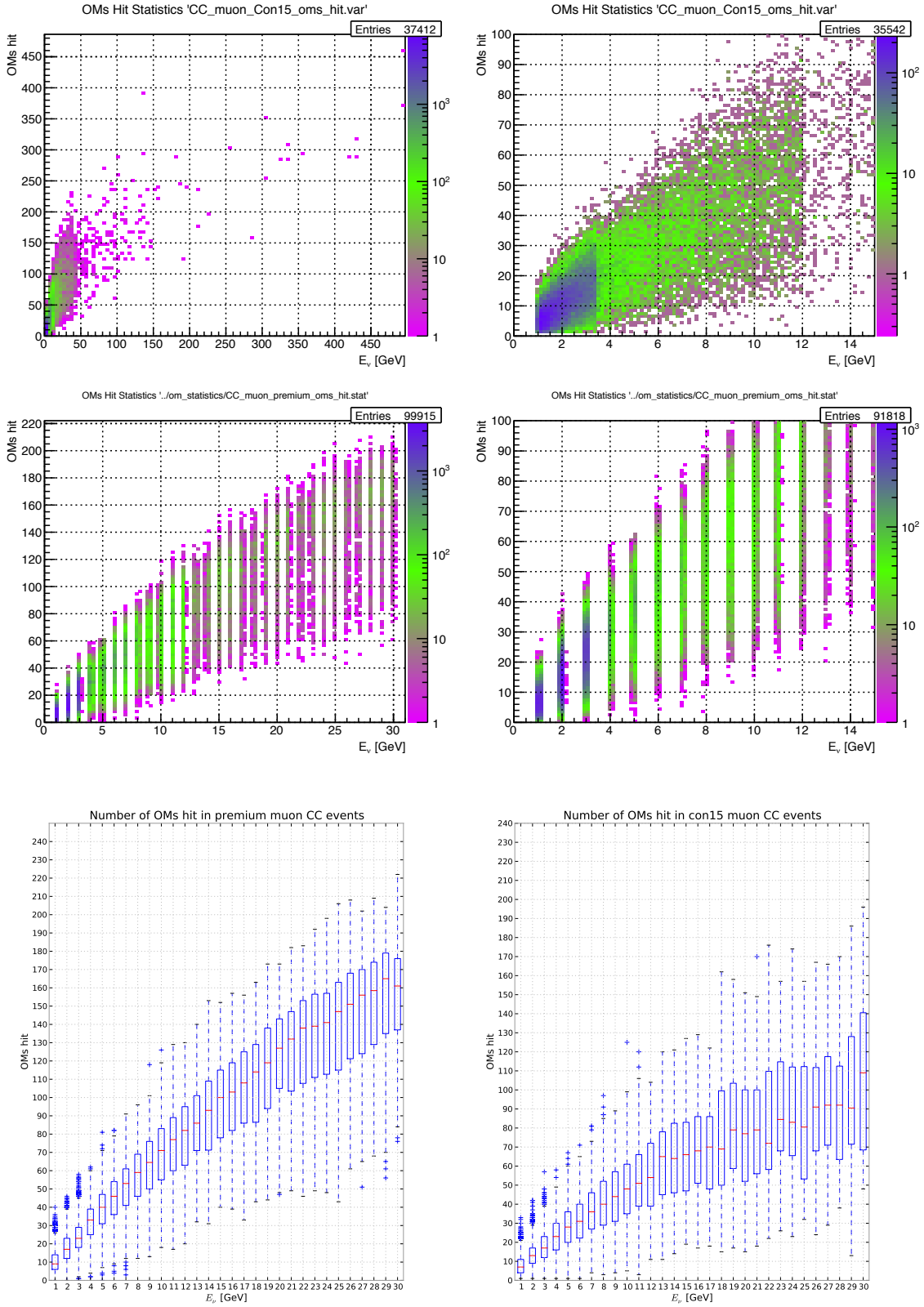

Figure 5.1: *Number of OMs hit per event versus the neutrino energy for 37k contained and 100k premium muon CC events without noise. The right plots show only events with* $E_\nu < 15\,\mathrm{GeV}$ *and less than 100 OM hits for better comparison. The bottom two box plots represent the statistics for each energy bin below 30 GeV.*

the first and third quartiles[1] are the lower and upper bounds of the box and the whiskers at the bottom and the top mark the minimum and maximum values within 1.5 IQR[2].

In contrast to muon CC events, the total number of OMs hit in electron CC events is significantly lower (about half as many) and even lower (nearly $\frac{1}{7}$) in electron NC events, as shown in Fig. 5.2. In case of electron CC events, the charged lepton track is shorter than in muon CC events and therefore fewer OMs are hit. In NC interactions, there is no such guaranteed charged lepton, so the Cherenkov light is produced by the hadronic shower resulting in a more compact photon emission volume and therefore a reduced OM coverage.

To sum up, a rule of thumb for the overall number of OMs hit in case of the ORCA reference detector for premium muon/electron CC and electron NC events is given by the formulae:

$$N_{OMs}^{CC,muon} \approx 7 \cdot \frac{E_\nu}{\mathrm{GeV}}$$
$$N_{OMs}^{CC,elec} \approx 4 \cdot \frac{E_\nu}{\mathrm{GeV}}$$
$$N_{OMs}^{NC,elec} \approx 1 \cdot \frac{E_\nu}{\mathrm{GeV}}$$

Since the neutrino's energy in CC interactions is deposited in an outgoing charged lepton and a hadronic shower (as discussed in section 2.2), it is worth to take a look at those parameters too.

The energy of the muon vs. the total number of OMs hit per event in contained and premium events is shown in Fig. 5.3.

There are slightly more OMs hit in the premium muon events, which is caused by different containment definitions and event selections. Premium events contain only up going neutrinos, so the Cherenkov light is mainly traveling upward. Since the ORCA OM has 19 PMTs looking downward and 12 upward, the expected total number of OMs hit is higher compared to contained events. In addition to that, the interaction vertex of *premium* events is located about 50 m away from the centre

[1] In descriptive statistics, the quartiles of a data set are defined by the three points that split up the data set into four equal groups, so that each group is holding a quarter of the data.

[2] IQR: InterQuartile Range or *midspread* is the difference of the upper and lower quartiles of a boxplot.

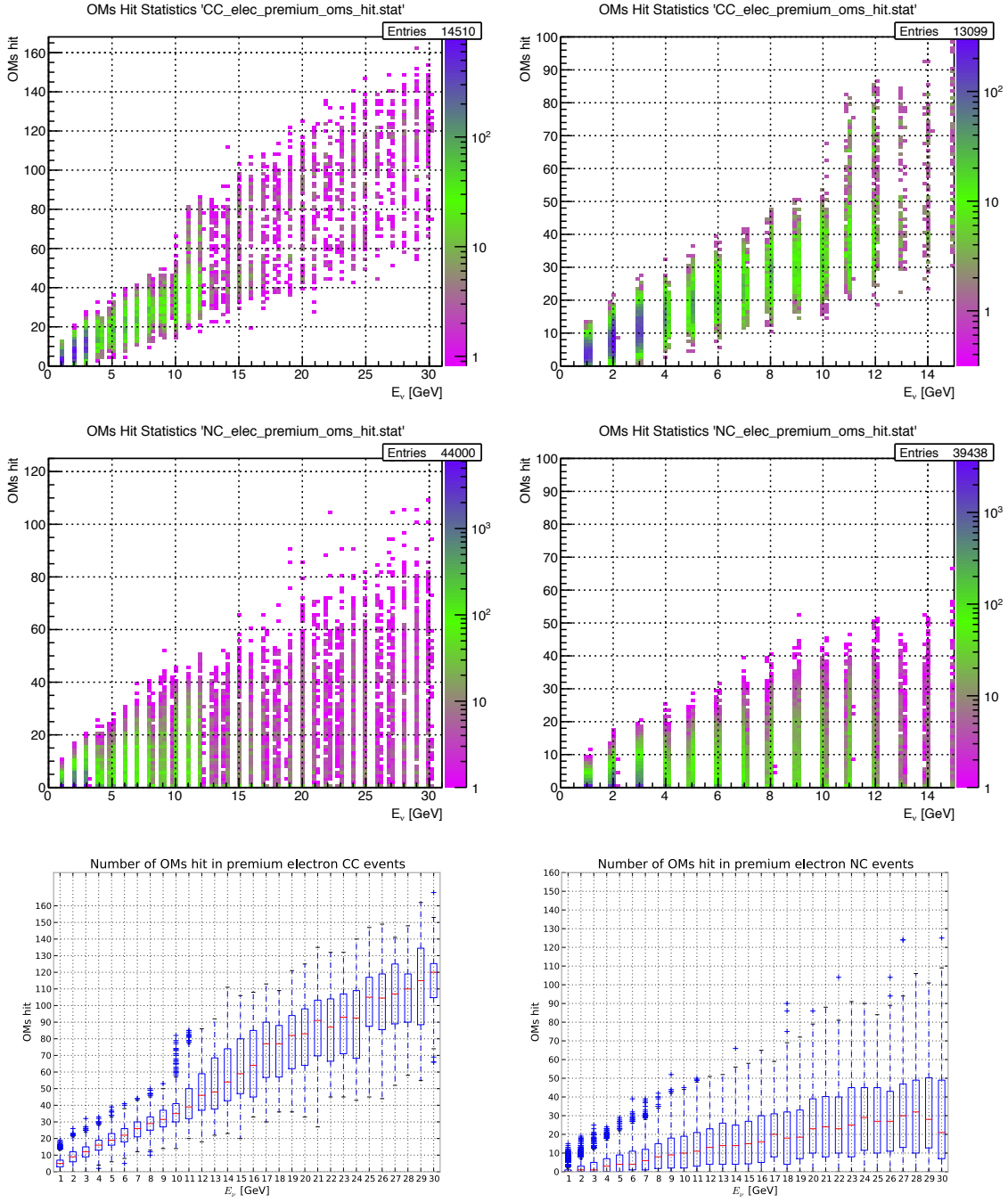

Figure 5.2: *Number of OMs hit per event versus the neutrino energy for 44k premium electron NC events without noise. The right plots show only events with* $E_\nu < 15\,\mathrm{GeV}$ *and less than 100 OM hits for better comparison.*

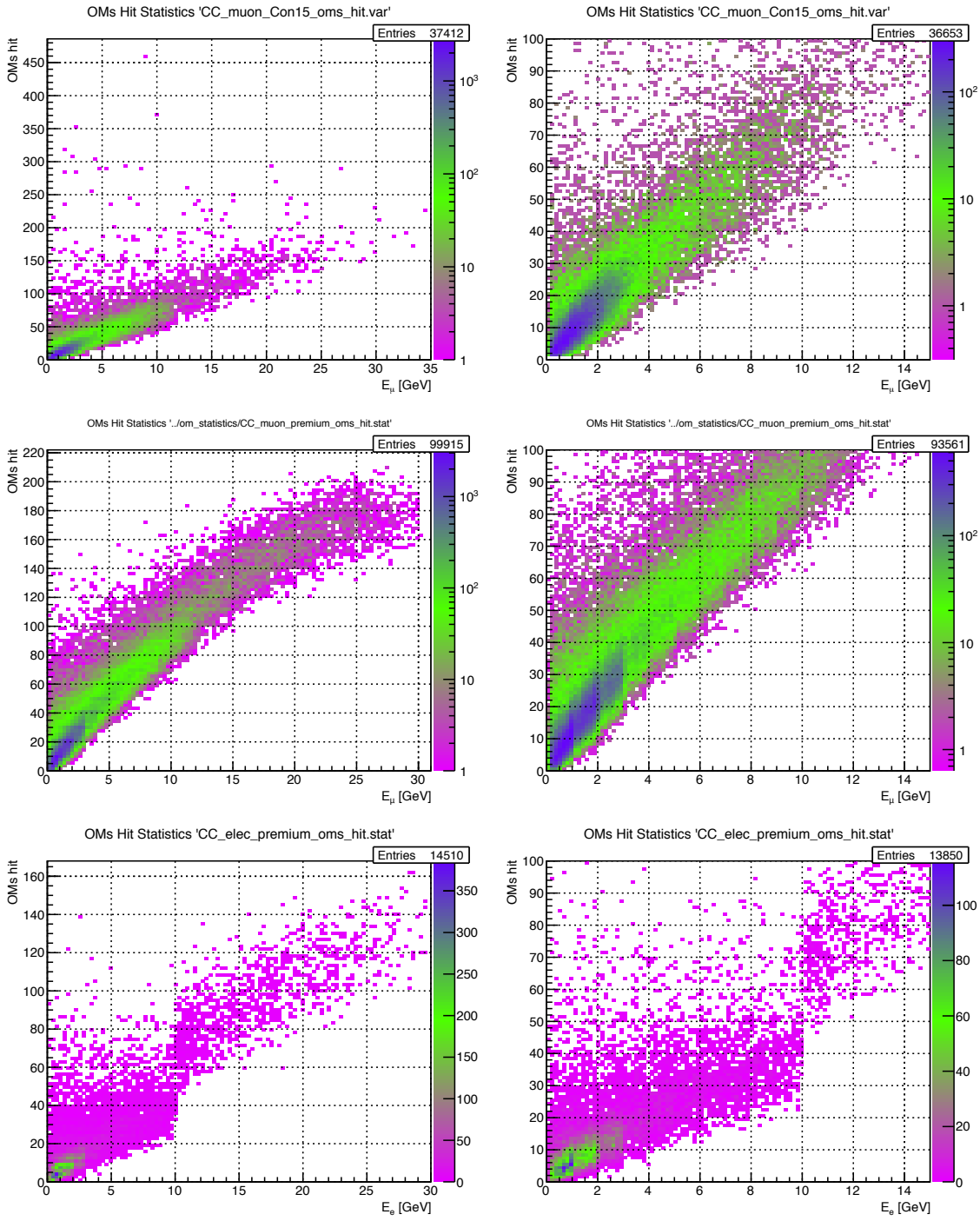

Figure 5.3: *Number of OMs hit per event versus the muon energy for 37k contained and 100k premium muon CC events and versus the electron energy for 14.5k premium electron CC events. The right plots show only events with* $E_\mu < 15\,\mathrm{GeV}$ *and less than 100 OM hits.*

of the detector and the muon's direction is pointing towards the centre (see 4.2), whereas the *contained*-condition is simply a muon track within the instrumented volume (see 4.1). In the contained-event selection, there are consequently events, where e.g., the muon is traveling very close to the outer bounds of the contained volume, while the worst case scenario for semi-premium events is when a muon *sticks through* the detector and its track-end is not contained. Since the muon energies are below $\approx 30\,\mathrm{GeV}$, the corresponding track lengths are via Eq. (2.8) not longer than $\approx 130\,\mathrm{m}$ and the muon tracks most likely are completely within the instrumented volume except it is traveling nearly horizontally to the ground. Therefore the average escape probability for photons is higher for contained events. The drop in the number of OMs hit for higher muon energies is also due to this effect.

The bottom two plots in Fig. 5.3 show the number of OMs hit per event in electron CC interactions. While the amount of OMs hit is also linearly rising with the neutrino's energy, the average number is only about one half compared to those in muon CC events. This is a consequence of the significantly shorter electron track as discussed earlier in section 2.2. The sudden increase of the counts above 10 GeV is due to the simulation procedure. Though *geasim* is configured to perform the full simulation of the particle tracking below 10 GeV, while above this threshold, the calculation is based on parametrisation. This obviously leads to an increase of photon numbers, which should be investigated further.

To visualise the effect of the neutrino energy split, the Bjorken-y variable (also referred to as inelasticity parameter)

$$y = 1 - \frac{E_\mu}{E_\nu} \ , \tag{5.1}$$

where E_μ is the total energy of the muon and E_ν the total energy of the incoming neutrino, is calculated for each event and plotted vs. the number of OMs hit. Fig. 5.4 shows the statistics for contained and premium muon CC events. The bottom two plots visualise the neutrino energy dependency of the Bjorken-y variable for both event types. In contained events, the energy split — at least for neutrino energies above $\approx 5\,\mathrm{GeV}$ seems to be randomly distributed to both the muon and the hadronic shower, whereas in premium events there is a tendency toward lower values, i.e., the muon is more likely to gain a larger fraction of the incoming neutrino's energy.

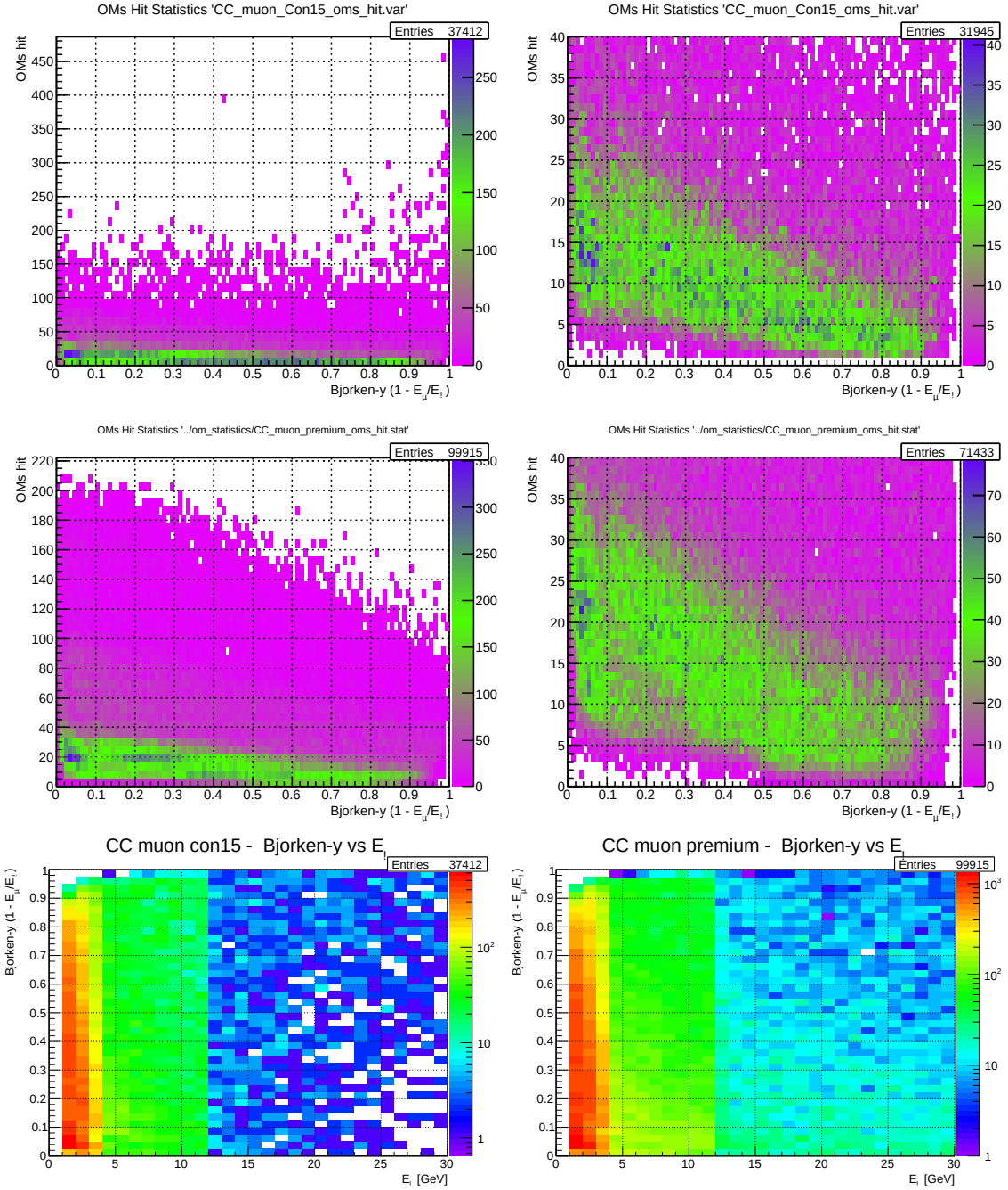

Figure 5.4: *Number of OMs hit per event versus Bjorken-y for contained and premium muon CC events. The bottom two plots show the Bjorken-y versus primary neutrino energy for both event types.*

Events where $y < 0.5$, i.e., where the main part of the energy is transferred to the muon, slightly more OMs are hit. The reason for this is that muons can travel larger distances compared to the dimensions of hadronic showers and therefore have a higher *OM coverage*.

The number of OMs hit is also correlated to the zenith angle of the incoming neutrino, since the ORCA OMs have more PMTs looking downward than upward (see 2.4) and moreover, the OMs aren't distributed on a regular grid. Fig. 5.5 shows the the number of OMs hit for premium muon and electron CC events ($90^{\circ} < \theta_Z < 180^{\circ}$). Although the effect is barely visible, a marginal rise of the median number of OMs hit is recognisable for increasing zenith angles. In case of electron NC events, this effect is not even noticeable due to the significantly lower OM hit rate.

5.1.2 Intra OM Pulses

Hits per OM

The number of hits per OM for premium muon CC events with and without *modk40* noise is shown in Fig. 5.6. The overall hit count with noise is important for future trigger algorithm development and optimisation, especially in case of online triggering. The average number of real physics hits on OMs as shown in the bottom plot, slowly increases with higher neutrino energies.

5.1.3 PMT Hit Coincidence Times

The hit time differences on PMT pairs within one OM are shown for premium muon CC events in Fig. 5.7 and for contained muon CC events in Fig. 5.7. The blue lines represent the signal only hits and the magenta lines are either pure noise hit pairs or mixed ones.

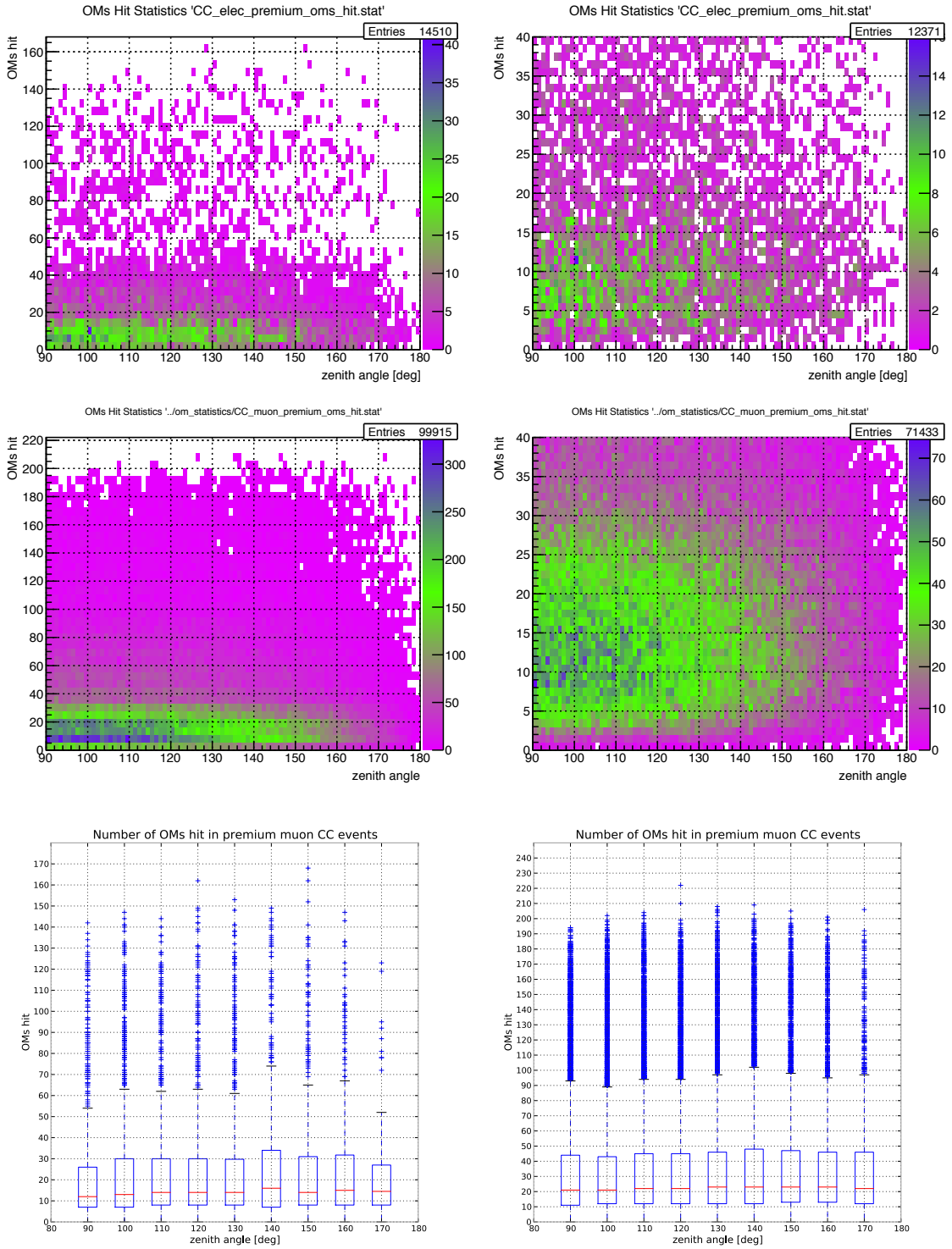

Figure 5.5: *Number of OMs hit per event versus the zenith angle for premium muon and electron CC events.*

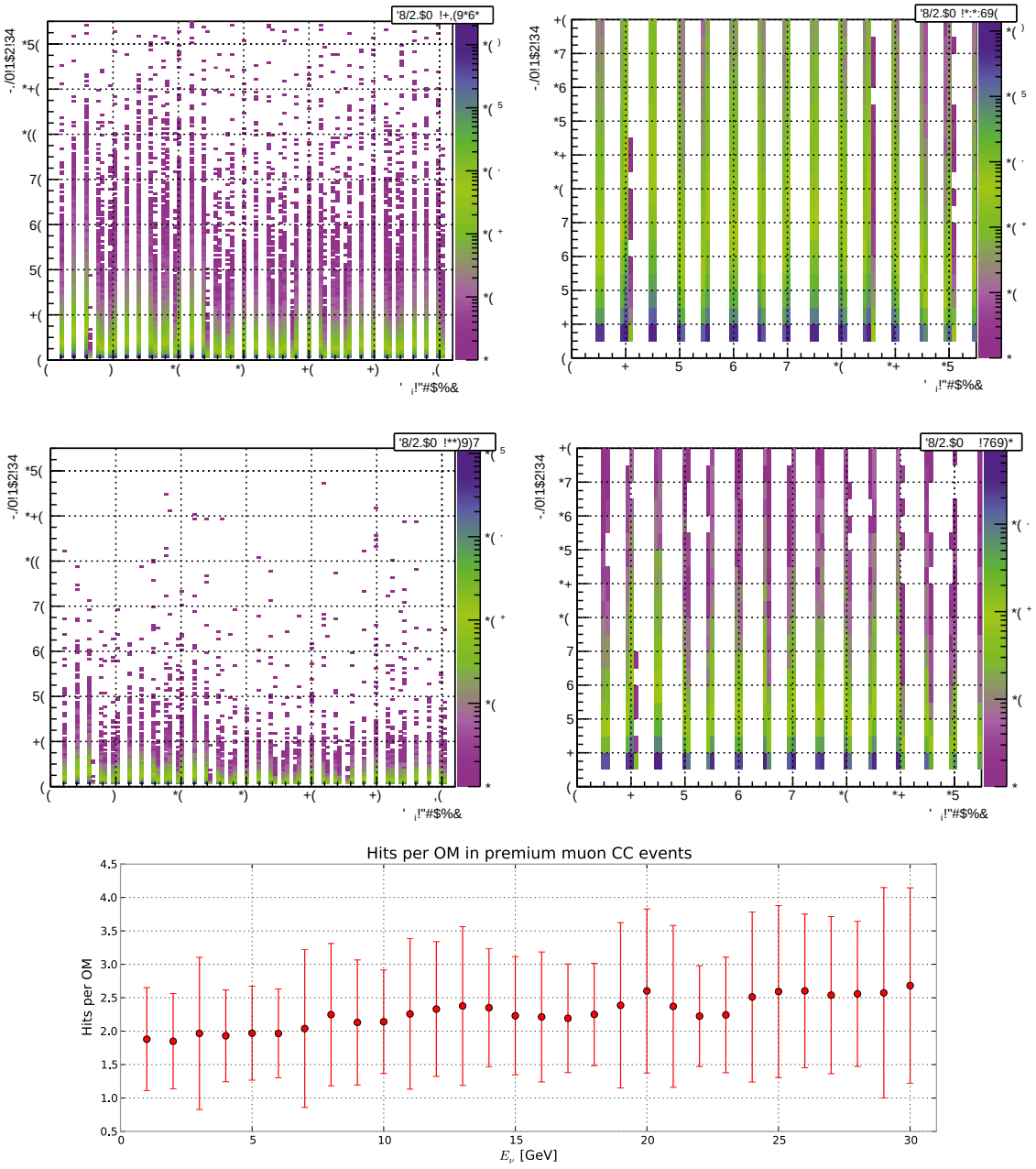

Figure 5.6: *Number of PMT hits per OM for muon CC premium events with (upper two plots) and without (middle two plots)* modk40 *noise. Only OMs with* $n_{hits} >= 1$ *are counted. The bottom graph shows the average number of hits per OM for events without noise.*

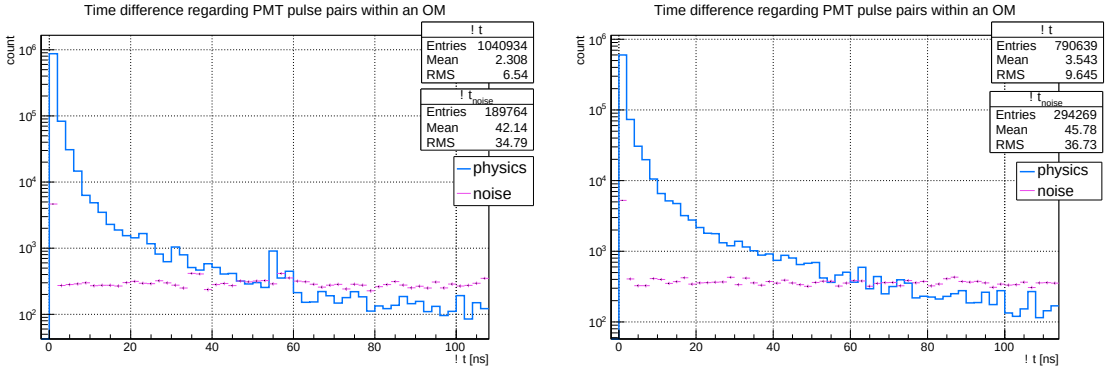

Figure 5.7: *Time differences of PMT hits (pair-wise) within an OM in contained (left) and premium (right) muon CC events.*

5.2 Trigger Algorithms

The trigger algorithms described in this section are implemented in Python[3] using the SeaTray framework, which is the primary software framework for ANTARES. It is based on the IceTray framework [9], developed by the IceCube[4] collaboration and is written in C++ with python bindings to allow rapid and efficient prototyping.

5.2.1 Trigger TnOMm

Triggers algorithms of type *TnOMm* trigger on events where at least n OMs have m pulses on PMTs correlated in space (neighboured or next-to-neighboured) and time ($! \ t < 10\,\text{ns}$).

The algorithm cycles through all OMs and fetches the PMT pulses on each of them. For each OM the possible combinations of pulse-pairs are calculated and examined for space and time correlations. Whenever the coincidence requirement for such a pulse-pair is fulfilled, the pulses information is saved and the PMT numbers put in a list, where each PMT number occurs only once. If the number of PMTs exceeds m, the OM is flagged. Finally the event is marked as triggered when at least n OMs were flagged, and last but not least the separately saved pulses are written to a new map within the event frame for later use.

Although this algorithm is not the most efficient one, it only takes $\approx 20\,\text{ms}$ to process

[3] http://www.python.org
[4] http://icecube.wisc.edu

an event under realistic noise conditions on my private computer[5]. The complexity of this algorithm regarding the PMT correlation part is (n is the number of PMTs):

$$\binom{n}{2} = \frac{n!}{2(n-2)!} = \frac{n!}{2 \cdot \frac{n!}{n(n-1)}} = \frac{n(n-1)}{2} = \mathcal{O}(n^2) \ , \tag{5.2}$$

which is good enough for prototyping purposes, since n hardly exceeds ≈ 100, in fact, $n < 40$ for $\approx 99.99\%$ of the OMs (see section 5.1.2). Another approach would be e.g., sorting the pulses by time (typically $\mathcal{O}(n \log n)$) and then traversing through the list while scanning for coincident pulses within the time window.

5.2.2 Trigger TnSm

This trigger algorithm triggers on events where at least n strings with m OMs on each of them are hit. Since this is a quite lose trigger condition, it should be used as a second level trigger, e.g., in combination with *TnOMm*. To reduce the computational time, separately saved triggered pulses from *TnOMm* can be used as input for *TnSm* extensions. In such a case, the trigger condition changes to: n strings with m OMs on each of them *having coincident pulses*.

[5]MacBook Pro mid 2010, 2×2.4 GHz Intel Core2Duo, 8 GB RAM

5.3 Evaluation of Trigger Performance

In this section the potential trigger response for different trigger configurations is presented. To get an overview of the trigger performance, several test conditions are investigated.

5.3.1 Purity

A trigger which selects every interesting physics event is worthless if it also fires on pure noise. The *purity* of a trigger is intended to give this property concrete values as it is defined by the fraction of not-triggered events on pure noise data:

$$\text{Purity} := 1 - \frac{N_{triggered}}{N_{events}} \tag{5.3}$$

The noise data is simulated by *modk40* with assumed noise conditions for the ORCA detector: an overall ^{40}K noise rate of 5 kHz and a coincidence rate[6] of 500 Hz.

Trigger Setup	$N_{triggered}$	Purity
T1OM2	6696	85.26%
T2OM2	484	98.93%
T3OM2	20	99.96%
T4OM2	1	99.998%
T5OM2	0	100%
T6OM2	0	100%
T3OM2+T1OM3	0	100%
T4OM2+T1OM3	0	100%
T2OM2+T1S2	12	99.97%
T3OM2+T1S2	1	99.998%
T4OM2+T2S2	0	100%

Table 5.1: *Purity of different trigger setups applied on 45432 pure* modk40 *noise events.*

Tab. 5.1 shows the purity for different trigger setups. At least four OMs with two hits on neighboured or next-to neighboured PMTs within 10 ns are needed to achieve a purity of nearly 100%. When triggering on three OMs with two correlated hits on each, an additional requirement of three coincident hits is needed for at least one of the OMs ⇒ the corresponding trigger setup is T4OM2+T1OM3. This trigger

[6] two hits within 20 ns on the same OM

configuration has a purity of 100% regarding the simulated data. Supplemental TnSm conditions can also be used on TnOMm triggers to improve their purity.

5.3.2 Trigger Efficiencies

To calculate the efficiency of different trigger setups, simulated events with preferably real physics conditions are taken and the fraction of triggered events is examined. The efficiency is therefore defined as

$$\text{Efficiency} := \frac{N_{\text{triggeredevents}}}{N_{\text{events}}} \ . \tag{5.4}$$

Triggering on CC Interactions

Fig. 5.8 shows the trigger efficiency of different TnOMn setups for contained and premium muon CC events. The fraction of triggered events for premium events is slightly higher than for contained events. This comes from higher OM hit rates in premium events as discussed in 5.1.1. The loosest trigger condition T1OM2 keeps nearly every event (>99%) where the neutrino's energy is $> 5\,\text{GeV}$, however the purity of this trigger is very poor (≈85%). As shown in 5.3.1, at least T4OM2 is required to suppress the fraction of triggered noise events below 0.01%. The efficiency of this trigger setup is at ≈80% on contained and ≈83% on premium events for neutrino energies above 5 GeV.

The most suitable triggering setup respecting the primary neutrino's energy is either T4OM2 or T3OM2+T1OM3. Both setups have a purity of at least 99.99% according to Tab. 5.1.

Fig. 5.9 shows the trigger efficiencies on premium electron CC events. The overall efficiency is worse compared to muon CC interactions, since the electron track is significantly shorter. T3OM2 has a 75% efficiency at $E_\nu \approx 5\,\text{GeV}$ and is with a purity of >99.9% the best trigger setup for this kind of events. Other trigger configurations only lower the efficiency without a significant increase of the purity.

Considering the efficiency with respect to the muon energy (see Fig. 5.10), T6OM2 already triggers slightly more than 80% of contained and about 90% of premium events for muon energies above 5 GeV. To increase the efficiency to near 100% at

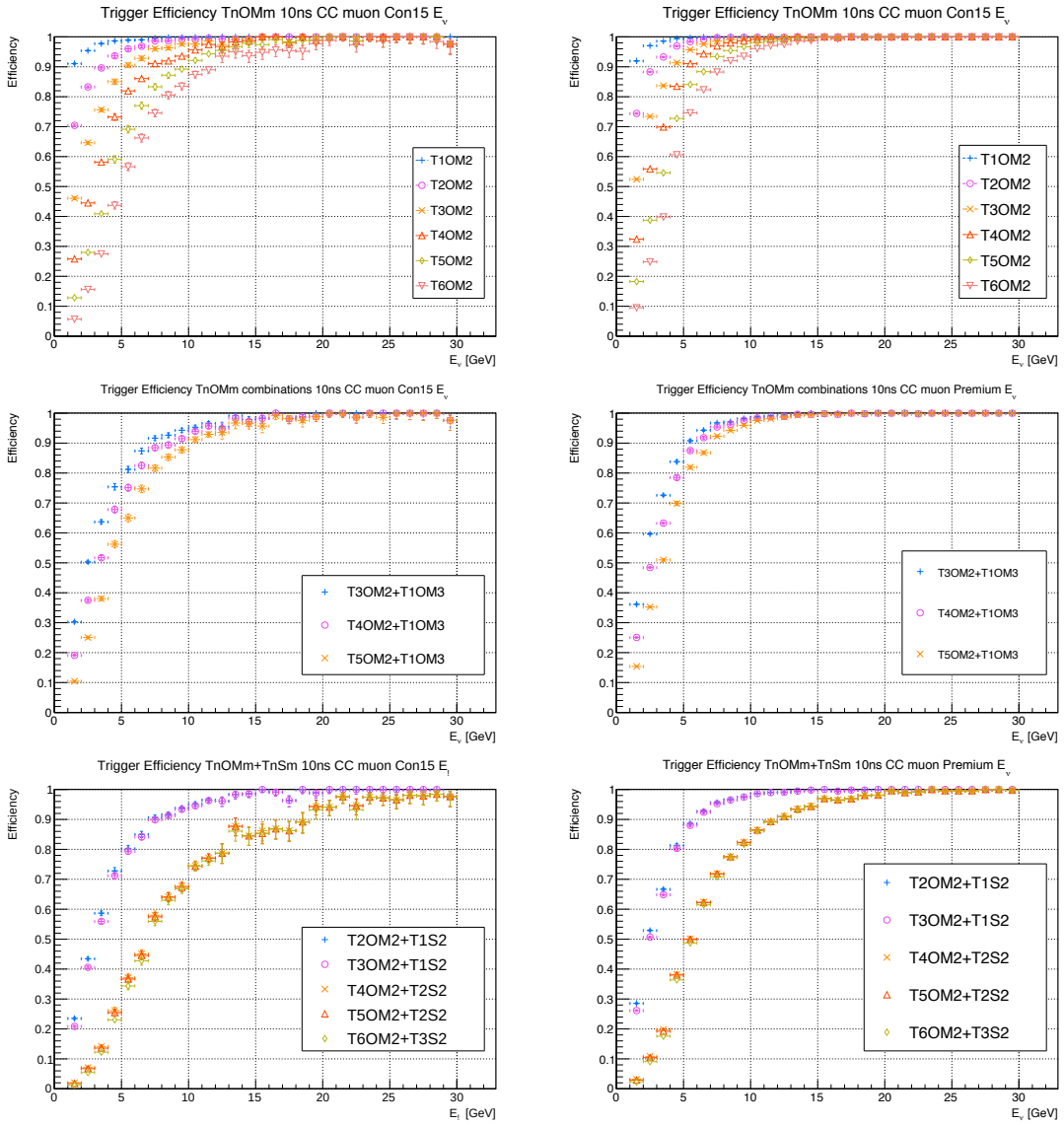

Figure 5.8: *Trigger efficiency of TnOMm and TnSm trigger configurations on 37k contained (left) and 100k premium (right) muon CC events with ^{40}K noise versus the primary neutrino energy.*

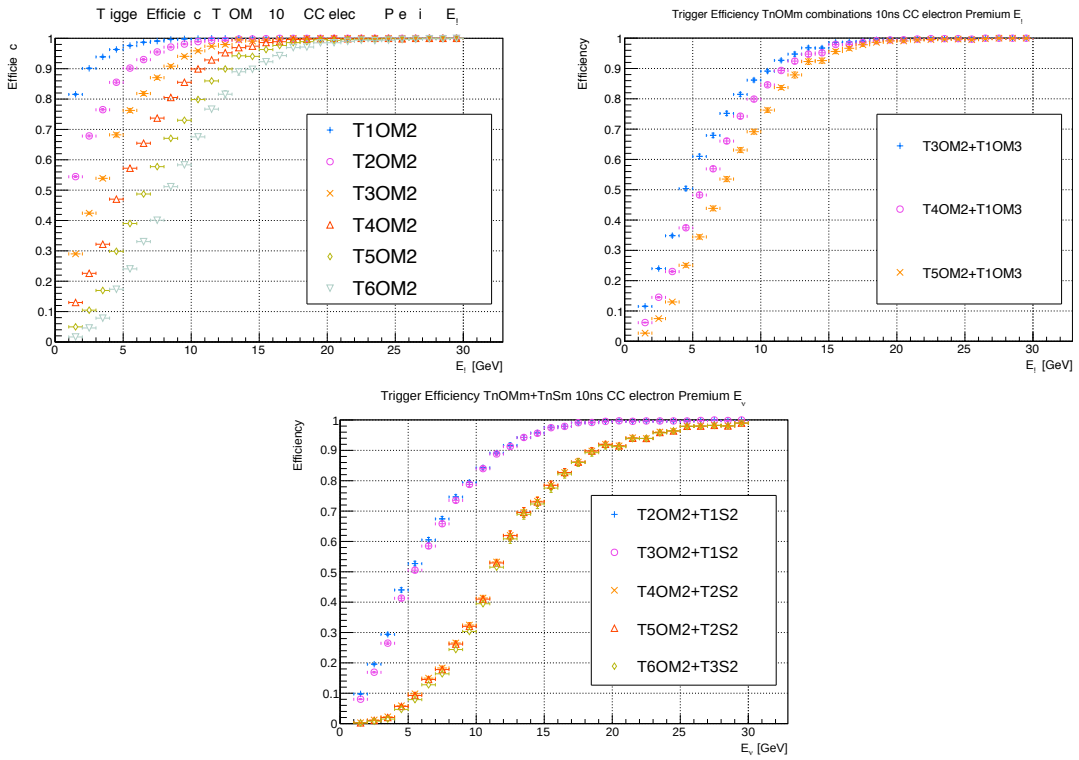

Figure 5.9: *Trigger efficiency of TnOMm and TnSm trigger configurations on 100k premium electron CC events with ^{40}K noise versus the neutrino energy.*

least T3OM2 or a looser condition is needed. Going further and requesting also a maximum purity, it turns out that T2OM2+T1S2 and T3OM2+T1S2 are the best candidates. They both provide a purity of >99.9% and an efficiency of ≈ 99%, due to the fact that muon tracks are longer than the shower and are more likely to hit at least two OMs on the same line. The error on efficiencies above 15 GeV in contained events increases due to poor statistics in that energy region.

Fig. 5.11 shows the trigger efficiency versus electron energy in premium electron CC events. The weird jump at 10 GeV is probably caused by *geasim* as already mentioned in 5.1.1 and shown in Fig. 5.3.

Fig. 5.12 shows the trigger efficiency on contained and premium muon CC events regarding the zenith angle. Although the low level trigger conditions introduced in this thesis are not meant to be explicitly sensitive to the muon track's direction (this will be the next step of trigger algorithm development), there is a noticeable variation of the efficiencies with respect to different zenith angles. One reason is that the ORCA OMs have more PMTs looking downward than upward, so the expected number of OMs hit subtly grows for larger zenith angles (see Fig. 5.5) and

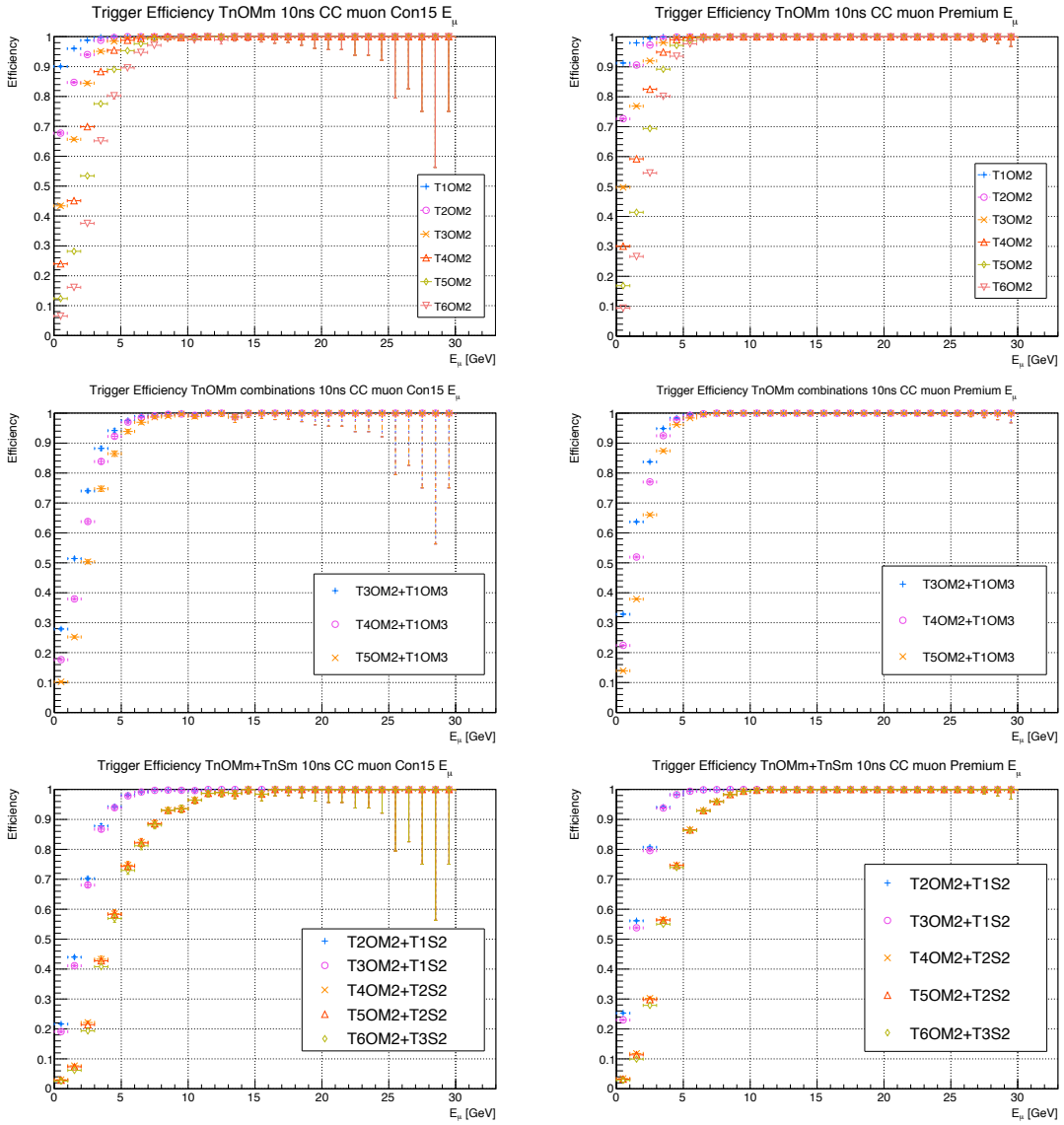

Figure 5.10: *Trigger efficiency of TnOMm and TnSm trigger configurations on 37k contained (left) and 100k premium (right) muon CC events with ^{40}K noise versus the muon energy.*

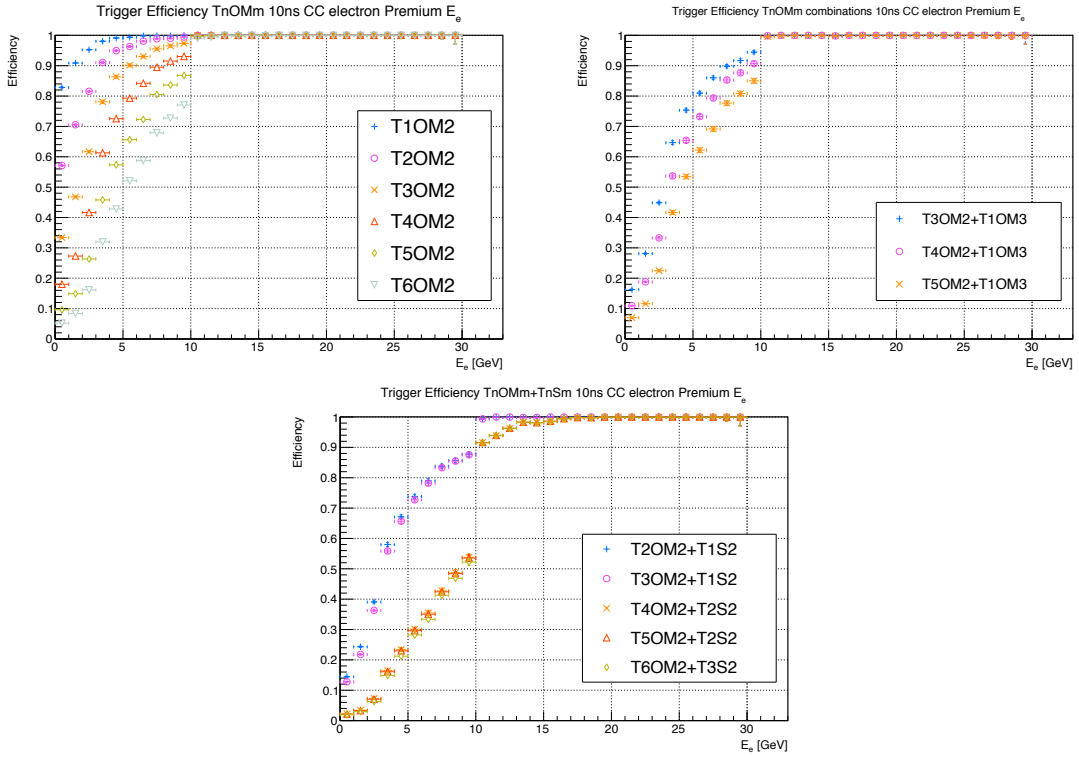

Figure 5.11: *Trigger efficiency of TnOMm and TnSm trigger configurations on 100k premium electron CC events with ^{40}K noise versus the electron energy.*

therefore the overall coincidence probability is a bit increased. The second reason is the irregular average OM density of the ORCA reference detector in the xy- and zy/zx-planes. The mean distance between the lines and therefore OMs in the xy-plane is about 16 m, whereas the OM distance on a string is 6 m. The Cherenkov cone of a muon traveling nearly horizontally through the detector volume, strikes to a certain degree more OMs than a muon with a vertical flight direction. Hence the probability of hitting multiple OMs on a string is better for zenith angles around 90°. The same is true for electron tracks in electron CC interactions (see Fig. **??**). This explains the efficiency drop drop above 160° for trigger setups where at least two strings with multiple OMs hit are required (T4OM2+T2S2, T5OM2+T2S2 and T6OM2+T3S2).

Fig. 5.13 shows the TnOMm trigger efficiency versus different Bjorken-y values in contained and premium muon CC events. The efficiencies drop consistently for $0 < y \lessapprox 0.8$ and increase for $0.8 \lessapprox y < 1$ to nearly 100%.

This strange increase is in fact a superposition of efficiencies in different energy ranges. A closer look on efficiencies of TnOMm combinations for several energy bins

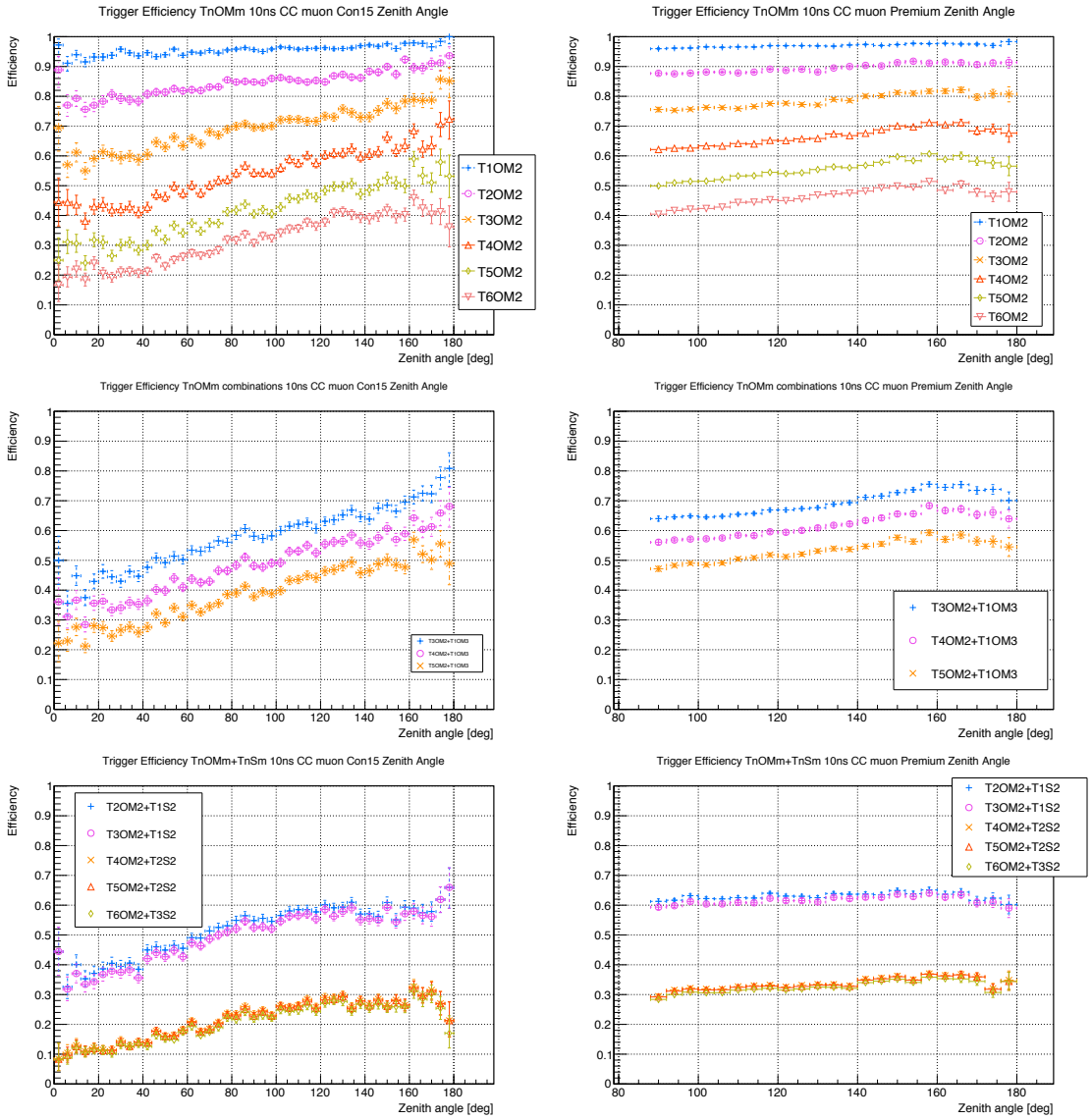

Figure 5.12: *Trigger efficiency of TnOMm and TnSm trigger configurations on 37k contained (let) and 100k premium (right) muon CC events with ^{40}K noise with respect to the zenith angle.*

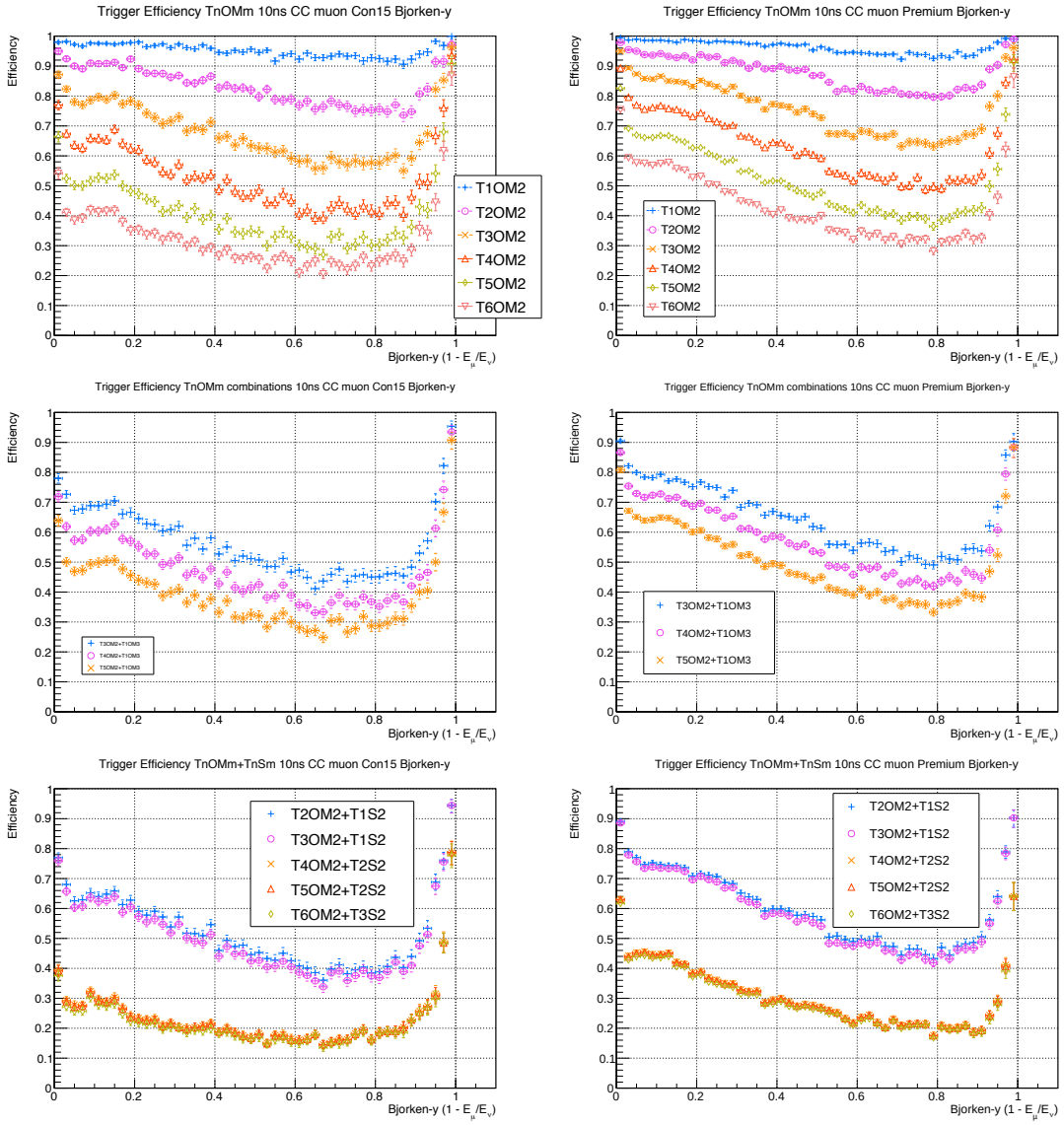

Figure 5.13: *Trigger efficiency of different TnOMm and TnSm setups on 100k premium muon CC events with ^{40}K noise and respect to Bjorken-y.*

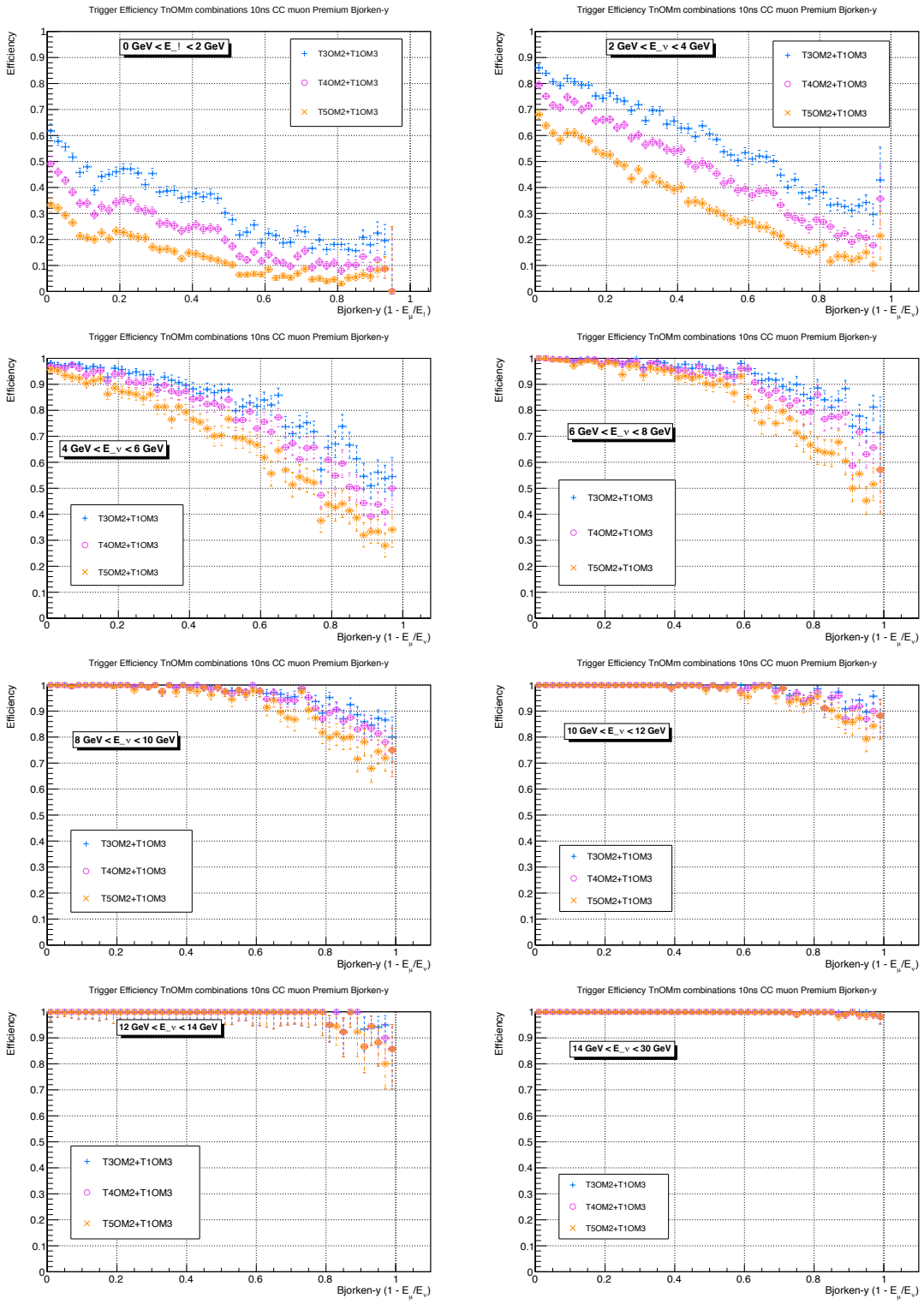

Figure 5.14: *Trigger efficiency of TnOMm combinations on 100k premium muon CC events with ^{40}K noise for different energy ranges.*

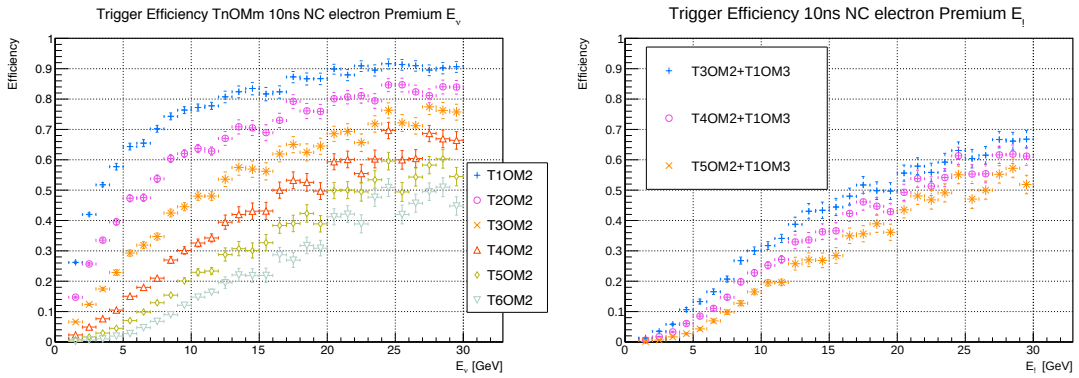

Figure 5.15: *Trigger efficiency of TnOMm and TnSm trigger configurations on 44k premium electron NC events with ^{40}K noise versus the incoming neutrino's energy.*

reveals a bit more, as shown in Fig. 5.14. Above $\approx 14\,\text{GeV}$, the efficiency is at nearly 100% and not depending on Bjorken-y, since the outgoing muon and the hadronic shower are both capable of producing enough Cherenkov light to fulfil the trigger requirements. On the other hand, at lower energies the effectiveness is decreasing with higher Bjorken-y values, while it also starts to fall below 100% for Bjorken-y near 0. The produced muon track in this energy regions is only a few meters long, not long enough to be triggered for sure. The overall Bjorken-y dependence of the trigger efficiency is then given by different weightings on each energy bin due to simulation systematics.

Triggering on NC Interactions

Neutral current interactions are harder to detect due to the fact that the outgoing neutrino is invisible to the detector, whereas in CC interactions the outgoing particle is a charged lepton and produces Cherenkov light. The sources of Cherenkov light in NC events are therefore charged particles in the hadronic shower part. The resulting low level trigger efficiencies for this type of neutrino interaction are depressingly low. Fig. 5.15 shows the trigger efficiencies with respect to the incoming neutrino's energy.

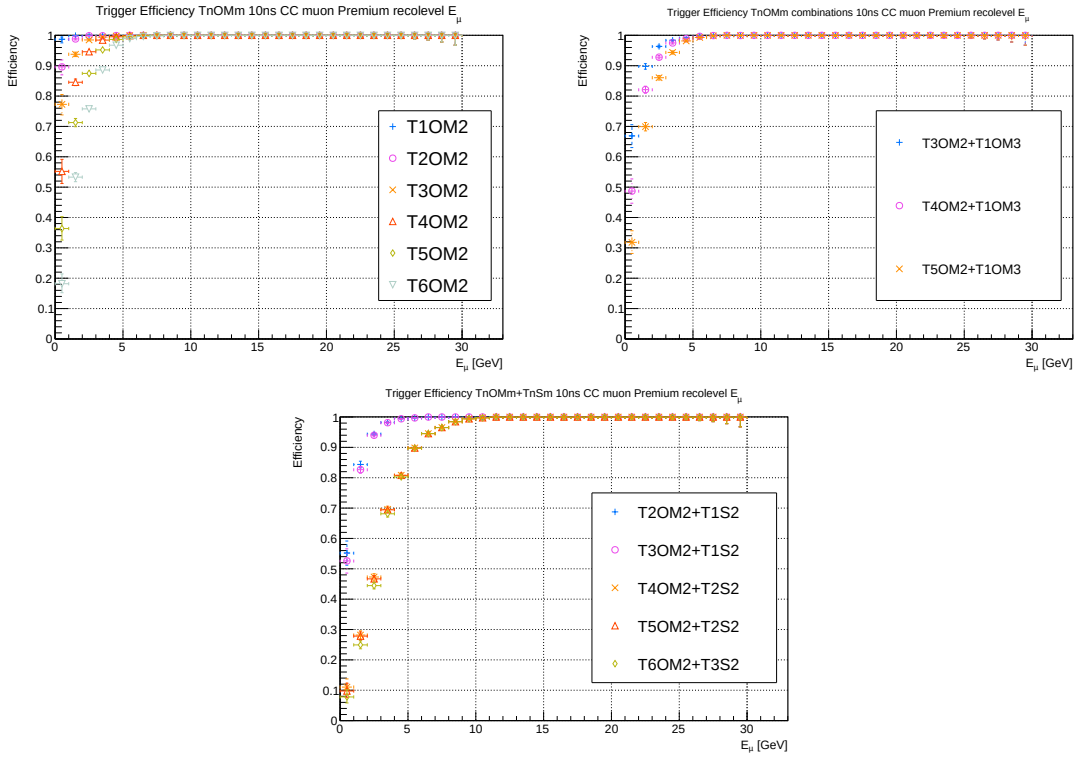

Figure 5.16: *Trigger efficiency of different TnOMm setups on 25k reconstructed premium muon CC events with ^{40}K noise with respect to the muon/neutrino energy, Bjorken-y and zenith angle. The selection criteria for reconstructed events was an angular distance of 5 deg or less.*

5.3.3 Trigger Efficiencies on Reconstruction Level

In the following, the trigger efficiencies on successfully reconstructed events (see 4.3) are presented. Fig. 5.16 shows the efficiencies of different trigger setups. Almost every trigger has nearly 100% efficiency regarding reconstructed events with muon energies above 5 GeV. The rather strict requirements of two or three strings with coincident hits on at least two OMs (T4OM2+T2S2, T5OM2+T2S2 and T6OM2+T3S2) have only about 85% efficiency at $E_\mu \approx 5\,\mathrm{GeV}$.

5.3.4 Trigger Rates

The trigger rate estimations in this section are determined by applying different trigger setups on atmospheric muon events generated by *MUPAGE*. In addition to that, *modk40* is used to mix in noise caused by ^{40}K decays. The events were created to simulate an overall lifetime of $\approx 25.7\,\mathrm{d}$ which allows estimations of trigger rates, i.e triggered events per time. Tab. 5.2 shows the rates for several trigger setups discussed in the previous sections.

Trigger Setup	$N_{triggered}$	percentage	trigger rate [Hz]
T1OM2	1603027	81.49%	17.32
T2OM2	1084252	55.12%	11.72
T3OM2	701970	35.69%	7.59
T4OM2	501211	25.48%	5.42
T5OM2	411174	20.90%	4.44
T6OM2	369900	18.80%	4.00
T3OM2+T1OM3	372793	18.95%	4.03
T4OM2+T1OM3	365903	18.60%	3.95
T5OM2+T1OM3	357018	18.15%	3.86
T2OM2+T1S2	427465	21.73%	4.62
T3OM2+T1S2	417885	21.24%	4.52
T4OM2+T2S2	321515	16.35%	3.47
T5OM2+T2S2	320947	16.32%	3.47
T6OM2+T3S2	265769	13.51%	2.87

Table 5.2: *Trigger rate estimations for different trigger setups on 1967052* MUPAGE *generated atmospheric muon events with* $\approx 25.7\,\mathrm{d}$ *lifetime.*

Chapter 6

Summary and Outlook

A study of low level trigger configurations based on Monte Carlo simulations for the ORCA reference detector has been presented. The efficiencies of several trigger setups were evaluated with respect to different event types and parameters.
It has been shown that the requirement of multiple OMs with neighboured or next-to-neighboured hits on PMTs within a 10 ns time window can be used to reduce the simulated noise background significantly, while still being efficient on accepting signal events. Furthermore, an estimation of trigger rates on atmospheric muon events has been calculated.

The next steps will be the development of higher level trigger algorithms which take into account the directionality of the PMTs and distances between strings and OMs. In addition to that, real data taken from first OM prototypes will be used to obtain a more accurate estimation on the real noise background including the bioluminescence rate, which therefore provokes a reevaluation of trigger efficiencies, rates and purities.

Erklärung

Hiermit bestätige ich, dass ich diese Arbeit selbstständig und nur unter Verwendung der angegebenen Hilfsmittel angefertigt habe.

Erlangen, den 31.07.2013

Tamás Gál

Bibliography

[1] Q R Ahmad and others. Measurement of the rate of nu/e + d –> p + p + e- interactions produced by B-8 solar neutrinos at the Sudbury Neutrino Observatory. *arXiv*, 87:071301, 2001. (Cited on page 4.)

[2] E Kh Akhmedov, Soebur Razzaque, and A Yu Smirnov. Mass hierarchy, 2-3 mixing and CP-phase with Huge Atmospheric Neutrino Detectors. *arXiv.org*, hep-ph, May 2012. (Cited on page 6.)

[3] N Agafonova et al. Observation of a first nu_tau candidate in the OPERA experiment in the CNGS beam. *arXiv.org*, hep-ex, June 2010. (Cited on page 4.)

[4] C. Andreopoulos et al. The GENIE Neutrino Monte Carlo Generator. *Nucl. Instrum. Meth.*, A614:87–104, 2010. (Cited on page 18.)

[5] P Antonioli, C Ghetti, E V Korolkova, V A Kudryavtsev, and G Sartorelli. A Three-dimensional code for muon propagation through the rock: Music. *arXiv*, 7:357–368, 1997. (Cited on page 20.)

[6] David J L Bailey. Km3 v2r1 : User guide. 2002. (Cited on page 20.)

[7] G Carminati, M Bazzotti, S Biagi, S Cecchini, T Chiarusi, A Margiotta, M Sioli, and M Spurio. MUPAGE: a fast atmospheric MUon GEnerator for neutrino telescopes based on PArametric formulas. *arXiv.org*, astro-ph.IM, July 2009. (Cited on page 19.)

[8] OPERA Collaboration. Search for nu_mu nu_e oscillations with the OPERA experiment in the CNGS beam. *arXiv.org*, hep-ex, March 2013. (Cited on pages 4 and 5.)

[9] T. DeYoung. IceTray: A software framework for IceCube. pages 463–466, 2005. (Cited on page 37.)

[10] A M Dziewonski and D L Anderson. Preliminary reference earth model. *Phys.Earth Planet.Interiors*, 25:297–356, 1981. (Cited on page 9.)

[11] H R Gallagher. Measurement of the atmospheric neutrino flavor ratio in Soudan 2. *Nucl.Phys.Proc.Suppl.*, 66:290–293, 1998. (Cited on page 18.)

[12] R L Graham. An Efficient Algorith for Determining the Convex Hull of a Finite Planar Set. *Information Processing Letters*, 1:132–133, January 1972. (Cited on page 23.)

[13] J. Beringer et al. (Particle Data Group). Review of Particle Physics, 2012-2013. Review of Particle Properties. *Phys. Rev. D*, 86(1):010001, 2012. (Cited on pages 4, 6, and 7.)

[14] D Jason Koskinen. Icecube-Deepcore-Pingu: Fundamental Neutrino and Dark Matter Physics at the South Pole. *Modern Physics Letters A*, 26(39):2899–2915, December 2011. (Cited on page 13.)

[15] Olga Mena, Hiroshi Nunokawa, and Stephen Parke. NOvA and T2K: The race for the neutrino mass hierarchy. *arXiv.org*, hep-ph, September 2006. (Cited on page 8.)

[16] S.P. Mikheev and A. Yu. Smirnov. Resonance amplification of oscillations in matter and spectroscopy of solar neutrinos. *Sov.J.Nucl.Phys.*, 42:913âĂŞ917, 1985. (Cited on page 7.)

[17] Simulations and HE Astrophysics Working Groups. Detector simulations for KM3NeT - ORCA Working Document 3.0. *KM3NeT Internal*, June 2013. (Cited on page 16.)

[18] A Yu Smirnov. The MSW effect and Solar Neutrinos. *arXiv.org*, hep-ph, May 2003. (Cited on page 8.)

[19] The Super-Kamiokande Collaboration. Evidence for oscillation of atmospheric neutrinos. *Physical Review Letters*, 81:1562–1567, 1998. (Cited on page 4.)

[20] Yung-Su Tsai. Pair Production and Bremsstrahlung of Charged Leptons. *Reviews of Modern Physics*, 46(SLAC-PUB-1365):815, 1974. (Cited on page 12.)

[21] L Wolfenstein. Neutrino oscillations in matter. *Phys. Rev. D*, 17(9):2369–2374, May 1978. (Cited on pages 6 and 7.)

List of Figures

1.1 Neutrino mass hierarchy 8

2.1 The NC neutrino interaction channel visible for neutrino telescopes. . 11
2.2 Neutrino CC interactions 12
2.3 An example footprint of the ORCA detector. 14
2.4 The optical module of the ORCA detector 14
2.5 The positions of the PMTs in the ORCA optical module. 15
2.6 Angles between PMTs in the ORCA optical module. 16
2.7 The quantum efficiency of the ORCA PMT. 16

4.1 Contained area/volume definition 22
4.2 Premium event definition 23
4.3 The generated energy spectra of the neutrinos in contained CC muon and CC/NC electron events. 24

5.1 OMs hit per muon CC event - neutrino energy 28
5.2 OMs hit per electron NC event - neutrino energy 30
5.3 OMs hit per muon/elecon CC event - muon/electron energy 31
5.4 OMs hit per muon CC event - Bjorken-y 33
5.5 OMs hit per muon/electron CC event - zenith angle 35
5.6 Number of PMT hits per OM for muon CC premium events 36
5.7 Time differences of PMT hits 37
5.8 Trigger efficiency on muon CC events regarding the primary neutrino's energy 41
5.9 Trigger efficiency on electron CC events regarding the neutrino energy 42
5.10 Trigger efficiency on muon CC events regarding the the muon energy 43
5.11 Trigger efficiency on electron CC events regarding the muon energy . 44
5.12 Trigger efficiency on muon CC events regarding the zenith angle . . . 45

5.13 Trigger efficiency on muon CC events regarding Bjorken-y 46
5.14 Trigger efficiency on muon CC events regarding Bjorken-y in different energy ranges 47
5.15 Trigger efficiency on electron NC events regarding the neutrino energy 48
5.16 Trigger efficiency of TnOMm on reconstructed premium muon CC events 49

List of Tables

5.1 Purity of different trigger setups 39
5.2 Trigger rates 50